Discrete Rotations on the Triangular Plane

Aydın Avkan

Submitted to the
Institute of Graduate Studies and Research
in partial fulfillment of the requirements for the degree of

Doctor of Philosophy
in
Mathematics

Eastern Mediterranean University
January 2022
Gazimağusa, North Cyprus

Approval of the Institute of Graduate Studies and Research

Prof. Dr. Ali Hakan Ulusoy
Director

I certify that this thesis satisfies all the requirements as a thesis for the degree of Doctor of Philosophy in Mathematics.

Prof. Dr. Nazım Mahmudov
Chair, Department of Mathematics

We certify that we have read this thesis and that in our opinion it is fully adequate in scope and quality as a thesis for the degree of Doctor of Philosophy in Mathematics.

Asst. Prof. Dr. Müge Saadetoğlu
Co-Supervisor

Prof. Dr. Benedek Nagy
Supervisor

Examining Committee

1. Prof. Dr. Hüseyin Aktuğlu
2. Prof. Dr. Rashad Aliyev
3. Prof. Dr. Cüneyt Bazlamaçcı
4. Prof. Dr. Gergely Kovács
5. Prof. Dr. Benedek Nagy
6. Assoc. Prof. Dr. Arif Akkeleş
7. Asst. Prof. Dr. Müge Saadetoğlu

ABSTRACT

There are various geometric transformations, e.g., translations, rotations, which are always bijections in the Euclidean space. Their digital counterpart, i.e., their digitized variants are defined on discrete grids, since most of our pictures are digital nowadays. Usually, these digital versions of the transformations have different properties than the original continuous variants have. Rotations are bijective on the Euclidean plane, but in many cases they are not injective and not surjective on digital grids. Since these transformations play an important role in image processing and in image manipulation, it is important to discover their properties. Neighborhood motion maps are tools to analyze digital transformations, e.g., rotations by local bijectivity point of view. In this thesis we show digitized rotations of a pixel and its 12-neighbors on the triangular grid. In particular, different rotation centers are considered with respect to the corresponding main pixel, e.g. edge midpoints and corner points. Angles of all locally bijective and non-bijective rotations are described in details. It is also shown that the triangular grid shows better performance in some cases than the square grid regarding the number of lost pixels in the neighborhood motion map. We also compare the bijectivity of the digitized rotations for the closest neighbors in all three regular grids. Rotations for every integer degree are studied for rotation centers at the corner, edgemidpoint and at the center of the pixels. The experiment proves that, when the center of rotation is the center or the corner of a main pixel, then, the triangular grid and the square grid have a better behaviour compared to the hexagonal grid.

Keywords: Digital rotations, Discrete motions, Non-traditional grids, Neighborhood motion maps, Lost pixels, Quality of images.

ÖZ

Öklid uzayında her zaman birebir ve örten olan çeşitli geometrik dönüşümler vardır; bunlara örnek olarak ötelemeler ve döndürmeler verilebilir. Günümüzde resimlerimizin çoğu dijital olduğundan, bunların dijitalleştirilmiş versiyonları; dijital varyantlar, ayrık ızgaralarda tanımlanmıştır.Genellikle, dönüşümlerin bu dijital versiyonları farklı özelliklere sahiptir. Döndürmeler Öklid düzleminde birebir ve örtendir ancak çoğu durumda dijital ızgaralarda birebir veya örten özellikleri sağlanmaz. Bu dönüşümler, görüntü işlemede önemli bir rol oynadığı için, belli özelliklerini keşfetmek önemlidir. Ana piksel komşularının hareket şemaları dijital dönüşümleri analiz etmek için bir araçtır, bunlara örnek olarak bölgesel birebir ve örtenlik özellikleri incelenebilir. Bu tezde, üçgen ızgara üzerinde ana pikselin ve 12 komşusunun dijitalleştirilmiş dönüşlerini inceledik. Ana piksel üzerinde, piksel merkezi, köşe noktaları ve kenar orta noktaları gibi farklı dönüş merkezleri düşünülmüştür. Tüm yerel birebir örten olan ve olmayan rotasyonlar ayrıntılı olarak açıklanmıştır. Komşu hareket haritasındaki kayıp piksel sayısı incelendiğinde bazı durumlarda üçgen ızgaranın kare ızgaradan daha iyi performans gösterdiği görülür. Bu tezde ayrıca her üç düzenli ızgarada en yakın komşular için dijitalleştirilmiş rotasyonların birebir örtenliği kıyaslanır. Her tamsayı açısı için, köşedeki, kenar orta noktadaki ve piksel merkezindeki dönüşler incelenir. Yapılan çalışma, dönüş noktası bir ana piksel merkezi veya köşesi olduğunda, üçgen ve kare ızgaraların altıgen ızgaraya göre daha iyi sonuç verdiğini göstermektedir.

Anahtar Kelimeler: Dijital döndürmeler, Komşu hareket şeması, Görüntü kalitesi, Piksel kaybı.

... Dedicated to AreL

ACKNOWLEDGMENTS

First of all I would like to thank my supervisor Prof. Dr. Benedek Nagy and my co-supervisor Asst. Prof. Dr. Müge Saadetoğlu for their support, encouragement and patience. I am so greatful to be part of the department of Mathematics at EMU. I give deep thanks to all the members.

To conclude, I cannot forget to thank my family and friends for all the unconditional support in this very intense academic year.

TABLE OF CONTENTS

LIST OF TABLES

LIST OF FIGURES

Chapter 1

INTRODUCTION

Rotations are fundamental transformations. In the Euclidean plane/space they are bijective and isometric. Image processing, computer vision and machine learning are among the main fields of artificial intelligence. As, nowadays, most of our data are digital, we usually have pictures on computers, on tablets, on smart phones, and on digital cameras. Rotations of these images are also very essential for multiple reasons. Consider an image taken with a phone in such a way that the horizontal line is not horizontal and the vertical line is not vertical. This is a scenario that happens very often. On the one hand, for a human observer to display the image in a better way on a computer or by a projector, she or he needs to rotate it accordingly. On the other hand, the rotation could be essential also when a computer vision or a machine learning algorithm wants to learn/identify the objects on the image. However, these images are digital, they are built up by pixels, thus a digital version of the rotation must be used. Rotations performed on a grid usually do not map the grid into itself, thus digitized rotations are equipped with a kind of rounding/digitizing operator. Considering the plane, there are three regular tessellations, namely the square, the hexagonal and the triangular ones, named after the regular polygon used to tile the plane. The traditional square grid is the most known and most used since it is studied already in the elementary school with its Cartesian coordinate system. However, the hexagonal and the triangular grids have more symmetry axes than the square grid. Actually, these two non-traditional grids are graph theoretical dual of each other, thus

there is a strong relation between them. They fit better also for the human eye than the square grid. Thus, there is a continuous effort to consider them also in applications connected to image processing. The hexagonal grid has a quite extensive literature, e.g., digital distance [1], tomography [2, 3], thinning [4, 5], skeletonization [6], digital rotations [7, 8] and also a book with various connected topics [9]. The triangular grid has a great advantage over the hexagonal grid, namely, the resolution of the images can be naturally changed by dividing a triangle pixel (trixel) to four equal ones, in a similar manner as a square can be divided into four smaller ones, or to join four neighbor pixels to a larger pixel of the same shape. This is impossible to do with hexagonal pixels (hexels). Various image processing techniques and algorithms are also performed on the triangular grid: tomography is considered in [10–12], digital distances are computed in [13], digital circles and disks are characterized in [14–16], mathematical morphology is presented in [17, 18], digital translations are described in [19], thinning algorithms and skeletonization are presented in [4–6, 20] and straight lines are characterized in [21]. While in the hexagonal grid every hexel has six neighbors, in the square grid each pixel has (four closest, so called cityblock neighbors and altogether) eight (so called chessboard) neighbors, in the triangular grid a trixel has twelve neighbors (including three closest ones). While the hexels and squares of the corresponding two grids have the same orientation, the triangular grid has two types of trixels, oriented in opposite ways. In this sense, the triangular grid seems more complicated than the other two mentioned grids, which may lead to some better properties in various applications, e.g., in approximating the Euclidean distance [22]. Rotations having very special angles can transform a grid into itself. Rotations that map the triangular grid into itself have been fully described in [23]. In this thesis rotations with arbitrary angle are analyzed on the triangular grid, especially by the neighborhood motion map. In general, bijectivity of a rotation is important as

this notion corresponds to the information loss in image processing. However, it is very easy to find a digitized rotation that is not bijective. The bijective digitized rotations were characterized on the square grid, by studying the non-bijective ones [24, 25]. In this thesis, extending the work presented in [26], we describe the neighborhood motion maps of the 12 neighborhood (that is the main pixel and its 12 neighbors) on the triangular grid. In [26], maps considering the closest neighborhood, that contains 3 neighbors, were presented. In our approach, for brevity, we consider the digitized rigid motions having no translation, i.e., the translation vector is the null vector. We note here that translations on the triangular grid are interesting themselves, since some of them are not bijective, and they are described in [19]. In the earlier mentioned works on the topic on other grids, e.g., in [7, 8], the center of the rotation was always the midpoint of a pixel. In our work, we use a more general setting, the center of the rotations will be at various points of the given (main) pixel: especially, we consider the midpoint, the corner points and the edge midpoints as rotation centers for both orientations of the trixels.

There is an interesting bivalence between the real (non-digital) and digital worlds. On one hand everybody celebrates the digital technology which allows us to make identical copies of pictures, videos, etc. without any loss of quality. On the other hand, there are various transformations, e.g., rigid motions, which can transform the input without loosing any information on the real, Euclidean geometry, but their digital counterpart, in general, does not have this property, e.g., rotating a digital image usually decreases its quality [27].

For instance, most of our smart devices can rotate our pictures by 90° since in this special angle, it is easy without decreasing the quality. In [28] it is mentioned that

"Rotation of rasters by angles other than 90 degrees is especially problematic since a sequence of consecutive rotations will distort the image". In practice, however, we may need such rotations: if for some reason, we take a picture in which the horizontal and vertical lines are not exactly oriented (which may easily happen if we use our hands for holding the smartphone), then we need very special algorithms and special care to rotate the picture for the correct angle to adjust the directions to the real directions.

Thus, it is an interesting experiment of combinatorial image analysis and discrete geometry to see what we can say about digital rotations on various grids. The properties of the underlying grid may have various effect on digital image processing, as properties of the images, and algorithms depend in many ways on the grid structure used. When one mentions 'digital plane' many people automatically consider the (traditional) square grid, as it is the most natural for most of the people due to square patterned exercise books used in schools and to the widely used Cartesian coordinate frame. However, there are various disadvantages of this grid, e.g., it has a topological paradox: the two diagonals of a usual chessboard are marked by different colors meaning that these two 'digital' lines cross each other without a crossing point. The hexagonal grid has no such paradox. This grid has also been used in various applications, also concerning digital images [2, 6, 9, 29–32]. The triangular grid is graph-theoretical dual of the hexagonal grid, and thus, sharing many symmetric properties with the hexagonal grid. These, also called, non-traditional grids have better symmetric properties with respect to the square grid. Various image processing algorithms are also developed for the triangular grid [2, 4–6, 12, 17–19, 32–34].

In this thesis, digital rotations are considered, which were already considered about 30 years ago by E. Andrés [35]. We recall that rotations in a grid usually do not map

the grid onto itself, thus digitized rotations are equipped with a kind of rounding/digitizing operator, thus the so-called digitized cell is used. Special angles of rotations map the grid to itself (depending both on the used grid and on the center of rotation), e.g., right angle (and its multipliers) for the square grid having center at the corner or at the center of a pixel. Further, for rotations around edge-midpoints, only rotations by the straight angle (180°) map the grid onto itself in each of the considered grid. Actually, we use the possible centers at the given locations, since these are the only possibilities to have a rotation that maps a regular grid onto itself. Rotations that map the triangular grid into itself have been described in [15, 23]. In general, bijectivity of a rotation is important as this notion is closely connected to the information loss (and thus, information preserving) of the transformation in image processing/manipulation as non-bijectivity implies information loss in the processed image. In [24, 25, 36] bijective and non-bijective digitized rotations on the square grid are specified, while in [8] the study is generalised to characterize the bijective rigid motions on the square grid by neighborhood motion maps both for the cityblock and chessboard-neighborhoods. Neighborhood motion map is a combinatorial technique used to analyse discrete/digital transformations. In [8], the hexagonal grid is involved to the study (based on neighborhood motion maps) and also some differences between the motions defined on the square and on the hexagonal grids are highlighted. In particular, in [8] authors gave a comparison of the loss of information (under the digitized rigid motion) between the two grids. To be more precise, they showed that given a digitized rigid motion on a finite subset of $\mathbb{Z}^2$, the loss of information on the hexagonal grid is less compared to those on the square grid. They computed this loss of information from the ratios between areas of non-injective zones and the remainder range. In [26], for both the square and the triangular grids, digitized rotations (with respect to different rotation centers) for each integer angle

between 0 and 360 degrees were considered. In these digitized rotations we examined the neighborhood motion maps of all 8 and 12 neighbors for the square and the triangular grids, respectively. As a result, in the square grid we realized that we have more pixel losses, at more angles, compared to the triangular grid.

Finally, in this thesis, in chapter 2 we formally recall and describe the three regular grids, their coordinate systems and digitized cells while in chapter 3 bijectivity of the neighborhood motion maps studied for triangular grid by considering all neighbors with the main trixel. We consider the digitized rigid motions by taking the translation vector as the null vector, but putting the rotation center to various positions, i.e., to the center, to the corner and to an edge midpoint of the main trixel. In chapter 4 we compare the bijectivity of all the three regular grids with respect to the closest neighbors [37]. Chapter 5 shows Applications with some experimental results and then we conclude the thesis by chapter 6.

Chapter 2

PRELIMINARIES

In this section we recall some basic concepts from the literature mentioned earlier. In this thesis, as usual, $\mathbb{R}$ denotes the set of real numbers, while $\mathbb{Z}$ is the set of integers. Consequently $\mathbb{R}^2$ denotes the Euclidian plane and $\mathbb{Z}^2$ denotes the square grid. All rotations will be taken in the positive (counterclockwise) direction. Further in this section, we provide some formal definitions.

2.1 Basic Definitions, Grids and Neighborhoods

First, we formally describe each of the three regular grids. We also show them on figure 2.1.

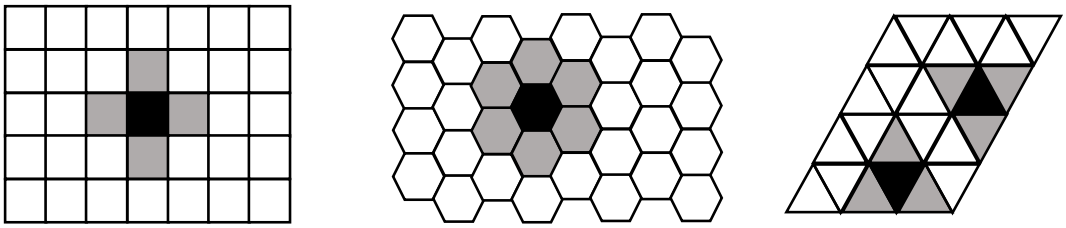

Figure 2.1: The square grid (left), the hexagonal grid (middle) and the triangular grid (right) showing the main pixels with their closest neighbors.

Definition 2.1: (Square Grid) A square grid $\mathbb{Z}^2$ is formed by a tessellation of $\mathbb{R}^2$ by squares of side length one unit. Actually we consider the center points of these squares.

Definition 2.2: (Triangular grid, trixel) A triangular grid $\mathscr{T}$ is a grid formed by a tessellation of $\mathbb{R}^2$ by regular triangles of side length $\sqrt{3}$ and of height 1.5 units. The pixels of the triangular grid are called trixels, abbreviated from triangular pixels. The grid is built up by trixels of two different orientations. With respect to these orientations we call them even $\triangle$ and odd $\triangledown$ triangles/trixels.

Definition 2.3: (Hexagonal grid) A hexagonal grid $\mathscr{H}$ is a grid formed by a tessellation of $\mathbb{R}^2$ by regular hexagons of side length $\frac{2}{\sqrt{3}}$. As above we consider the center points of these hexagons, that is to say, the points of the underlying lattice $\Lambda = 2\mathbb{Z} \oplus \mathbb{Z}\omega$ where $\omega = -1 + \sqrt{3}i$. The elements of Λ are called *Eisenstein* integers; they are the complex numbers of the form $\alpha = a + b\omega$ where $a, b \in \mathbb{Z}$, see definition 2.6. We will call the pixels of the hexagonal grid *hexels*, referring to [31].

In this thesis, for our experiment, we use the Cartesian coordinate system for the three grids, together with the triplet coordinate system for the triangular and the hexagonal grids as we shall explain here. In [15, 34, 38, 39], a three-coordinate-valued system of zero-sum triplets is used to describe the hexagonal grid keeping the triangular symmetry of the grid. In figure 2.2, the first coordinate value is increasing in the right upward direction, the second value is increasing in the downward direction, and finally the third one is increasing in the left-upward direction [38, 40]. The triangular grid has similar symmetry to the hexagonal grid. Therefore, in [15, 41], a coordinate system with zero-sum and one-sum triplets are used to describe this grid. The angle between any two of the three coordinate axes is 120° in both of the grids.

Definitions below give the Cartesian coordinate system we use for the three grids. However, the origin $(0,0)$ of the coordinate system changes with respect to the center

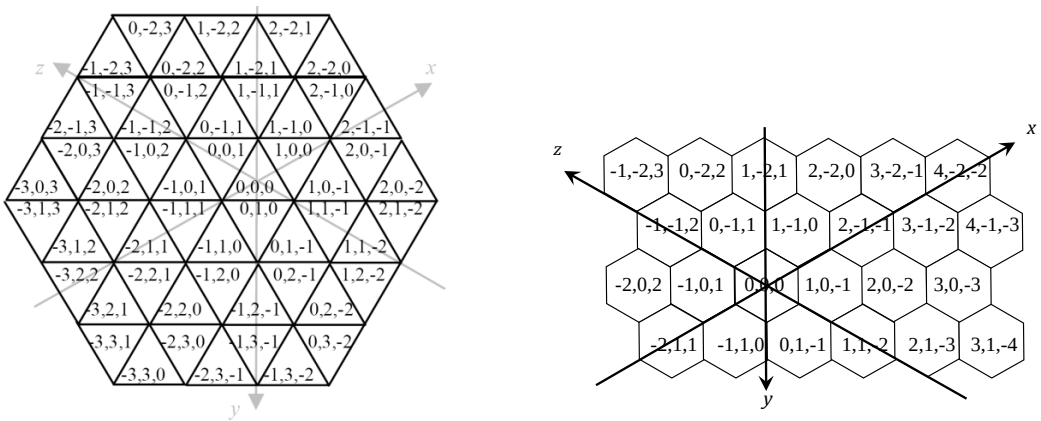

Figure 2.2: The triplet coordinate system for the triangular grid (left) and the hexagonal grid (right).

of the rotation. Formally, we define them as follows:

Definition 2.4: (Coordinate systems of the square grid) Let $\mathscr{S}_c$, $\mathscr{S}_m$ and $\mathscr{S}_e$ denote the set of the midpoints of the squares with respect to the center of rotations which is the corner, the center and the edge mid-point of the main pixel, respectively. Then $\mathscr{S}_m = \mathbb{Z}^2$, $\mathscr{S}_c = \mathbb{Z}^2 + (\frac{1}{2}, \frac{1}{2})^t$, and $\mathscr{S}_e = \mathbb{Z}^2 + (0, \frac{1}{2})^t$. The coordinate systems $\mathscr{S}_c$ and $\mathscr{S}_e$ can be obtained by applying the corresponding translation vector to $\mathscr{S}_m$.

Definition 2.5: (Coordinate system of the triangular grid) Let $\mathscr{T}_c, \mathscr{T}_m$ and $\mathscr{T}_e$ denote the set of the midpoints of the trixels with respect to the center of rotations which is the corner, the center and the edge mid-point of the main trixel, respectively. The notations $\mathbb{E}$ and $\mathbb{O}$ below denote the sets of the midpoints of the two different orientation (the even and the odd) trixels, respectively:
$\mathscr{T}_m = \mathbb{E} \cup \mathbb{O}$ where $\mathbb{E} = \mathbb{Z}(\sqrt{3}, 0)^t \oplus \mathbb{Z}\left(-\frac{\sqrt{3}}{2}, \frac{3}{2}\right)^t$ and $\mathbb{O} = \mathbb{E} + \left(\frac{\sqrt{3}}{2}, \frac{1}{2}\right)$ where the second vector denotes the translation vector required to give the coordinates of all the odd trixels. The coordinate systems $\mathscr{T}_c$,and $\mathscr{T}_e$, can be obtained by applying the translation vectors $\left(-\frac{\sqrt{3}}{2}, -\frac{1}{2}\right)^t$ and $\left(0, -\frac{1}{2}\right)^t$ to $\mathscr{T}_m$, respectively.

Definition 2.6: (Coordinate systems of the hexagonal grid) Let $\mathscr{H}_c$, $\mathscr{H}_m$ and $\mathscr{H}_e$ denote the set of the midpoints of the hexagonal pixels (hexels) with respect to the center of rotations which is the corner, the center and the edge mid-point of the main hexagonal pixel, respectively. Then $\mathscr{H}_m = \mathbb{Z}(0,2)^t \oplus \mathbb{Z}(\sqrt{3},-1)^t$. The coordinate systems $\mathscr{H}_c$ and $\mathscr{H}_e$ can be obtained by applying the translation vectors $(\frac{1}{\sqrt{3}},1)^t$ and $(0,1)^t$ to $\mathscr{H}_m$, respectively.

Definition 2.7 (rigid motions on $\mathbb{R}^2$): Rigid motions on $\mathbb{R}^2$ are bijective distance and angle preserving maps (isometries). They consist of translations, rotations and their compositions. Ŭ: $\mathbb{R}^2 \to \mathbb{R}^2$ where $x \to Rx+t$ will be the generalized form of the rigid motion, where the rotation matrix is $R = \begin{pmatrix} cos\theta & -sin\theta \\ sin\theta & cos\theta \end{pmatrix}$, and t is the translation vector (t_1,t_2). In this thesis, we do not use translation, thus $t = (0,0)^t$. Consequently we put the origin of our coordinate system to the center of the rotation at each case and thus, the rotation is about the origin. Let us consider rigid motions on $\mathbb{Z}^2$. If we apply the rigid motion to a point with integer coordinates, the resulting image may not have integer coordinates. Therefore we need to define digitized rigid motions which map $\mathbb{Z}^2$ to $\mathbb{Z}^2$.

Definition 2.8: (Digitized rigid motion). Digitized rigid motion U is the composition of two functions; the rigid motion Ŭ restricted to the domain $\mathbb{Z}^2$, denoted by $\check{U}_{\mathbb{Z}^2}$, and the digitization operator $D : \mathbb{R}^2 \to \mathbb{Z}^2$, where digitization operator maps $\mathbb{R}^2$ to $\mathbb{Z}^2$. Therefore, the digitized rigid motions are defined by U:$\mathbb{Z}^2 \to \mathbb{Z}^2$, where $U = D \circ \check{U}_{\mathbb{Z}^2}$.

Definition 2.9: (Neighbor relations) Triangular grid has 3 types of neighbor relations. Two trixels are neighbors if they share at least one point on their border. The triangular grid has three types of neighbor relations according to the Euclidean

distance of the midpoints of the corresponding trixels. Each pixel has three 1-neighbors (side neighbors), nine 2-neighbors (side ones counted as well) and twelve 3-neighbors (the side and 2-neighbors counted as well), see Figure 2.3. 3-neighbors that are not 2-neighbors are called strict 3-neighbors, while 2-neighbors that are not 1-neighbors are called strict 2-neighbors. The central trixel is usually referred as the main pixel. While in the hexagonal grid every hexel has six neighbors, in the square grid each pixel has four closest, (so-called cityblock) neighbors and altogether eight (so called chessboard) neighbors. Figure 2.1 shows the main pixel with its closest neighbors in all 3 regular grids.

In this thesis, for brevity, we use the Cartesian coordinate system for the triangular grid. However, the origin $(0,0)^t$ of the coordinate system changes with respect to the center of the rotation. Formally, we define them as follows:

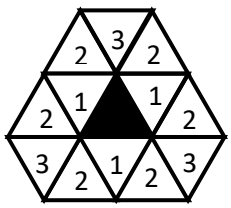

Figure 2.3: Neighborhood relation: various types of neighbors of the main trixel (black) are shown.

Definition 2.10: (Digitized rotation on the square grid) Digitized rotation $U_{\mathscr{S}}$ is the composition of two functions, the rigid motion $\breve{U}_{\mathbb{Z}^2}$ restricted to the domain $\mathbb{Z}^2$ and the digitization operator $D_{\mathscr{S}} : \mathbb{R}^2 \to \mathbb{Z}^2$. Therefore, the digitized rotation is defined by $U_{\mathscr{S}} : \mathbb{Z}^2 \to \mathbb{Z}^2$, where $U_{\mathscr{S}} = D_{\mathscr{S}} \circ \breve{U}_{\mathbb{Z}^2}$.

Definition 2.11: (Digitized rotation on the triangular grid) A digitized rigid motion U on the triangular grid is the composition of the rigid motion $\breve{U}$ restricted to the domain

$\mathscr{T}_i$ denoted by $\breve{U}_{\mathscr{T}_i}$ where $i \in m,c,e$, and the digitization operator on the triangular grid $D : \mathbb{R}^2 \to \mathscr{T}_i$. Thus, the digitized rigid motions on the triangular grid are defined by $U : \mathscr{T}_i \to \mathscr{T}_i$, where $U = D \circ \breve{U}_{\mathscr{T}_i}$.

Definition 2.12: (Digitized rotation on the hexagonal grid) A digitized rotation $U_{\mathscr{H}_i}$ on the hexagonal grid is the composition of the rigid motion $\breve{U}$ restricted to the domain $\mathscr{H}_i$, denoted by $\breve{U}_{\mathscr{H}_i}$, $i \in \{m,c,e\}$, and the digitization operator on the hexagonal grid $D_{\mathscr{H}_i} : \mathbb{R}^2 \to \mathscr{H}_i$. Thus, the digitized rotations on the hexagonal grid are defined by $U_{\mathscr{H}_i} : \mathscr{H}_i \to \mathscr{H}_i$, where $U_{\mathscr{H}_i} = D_{\mathscr{H}_i} \circ \breve{U}_{\mathscr{H}_i}$.

While in the square grid, simple rounding operation can be used for digitization, it is not so straightforward to define the digitization operation D on the triangular grid. In the following subsection we describe the digitized cell for the triangular grid.

2.2 Digitized Cells on the Three Grids

Since rotations and in general geometric transformations do not map a grid onto itself, we need so called digitization operators that map the plane to the used gridpoints.

Definition 2.13: (Digitized cell of the square grid) In square grid, we define the digitization operator, i.e., the digitized cell as follows. Given the Cartesian coordinates (x,y), of a point, we use the rounding operator, or more precisely, the formulas $\lfloor x+0.5 \rfloor$ and $\lfloor y+0.5 \rfloor$, with the floor functions, are used. We will denote this digitization operator for the square grid by $D_{\mathscr{S}}$. In the square grid, a simple rounding operation can be used for digitization, however it is not very easy to define the digitization on the triangular grid.

Definition 2.14: (Digitized cell of the triangular grid) We use digitized cell to map

any point of the plane to a trixel, e.g., the image of the midpoint of a trixel after a rotation is mapped to the center of the trixel the image belongs. If the midpoint of a given pixel falls inside of any trixel after the digitized rotation, then the image clearly belongs to that trixel, and the mapping is clear, see Figure 2.4, left for an example.We now consider the cases when the image is on the edge of a trixel, i.e., the midpoint of a trixel gets mapped by the rotation to a point on an edge. We define the digitized cell by showing which edges and corners belong to which trixel. First we consider the cases when the (image) point is not a corner, but on an edge. If the (image) point lies on any diagonal line (grid line with the equation $y = -\sqrt{3}x + (3n+1)$, $n \in \mathbb{Z}$ in $\mathscr{T}_m$) then it is mapped to the corresponding odd triangle, if it lies on any horizontal grid line (with equation $y = \frac{3}{2}n + 1, n \in \mathbb{Z}$ in $\mathscr{T}_m$), or anti-diagonal line (grid line with the equation $y = \sqrt{3}x + (3n+1), n \in \mathbb{Z}$ in $\mathscr{T}_m$) then it is mapped to the corresponding even triangle. If the (image) point is mapped to the left corner of an even pixel (which lies between the anti-diagonal and the horizontal grid lines corresponding to this pixel), then we map it to that even pixel (Figure 2.4, right). With respect to this if the origin is taken to be the center of an even or an odd trixel, then the digitized cell can mathematically be described as follows. For an even trixel it is the region $\mathscr{E}_D = \{y \leq \sqrt{3}x + C_1\} \cap \{y < -\sqrt{3}x + C_2\} \cap \{y \geq \frac{3}{2}k + 1\}$ and for an odd trixel, it is the region $\mathscr{O}_D = \{y \geq -\sqrt{3}x + C_3\} \cap \{y > \sqrt{3}x + C_4\} \cap \{y < \frac{3}{2}k + 1\}$, where $C_i = 3m + 1$ with $m, k \in \mathbb{Z}$. Generally, the digitization operator in triangular grid will be denoted by $D_{\mathscr{T}}$. For the other 2 coordinate systems digitized cell is defined in a similar way based on the grid lines with the same slope.

In the next section, as the main part of the thesis, we analyze the bijective property of digitized rigid motions, actually rotations, with all angles $(0^\circ \leqslant \theta \leqslant 360^\circ)$ We consider three possible choices for the center of the rotation is midpoint of a trixel, the corner

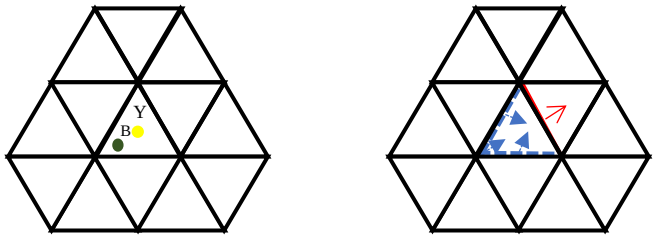

Figure 2.4: B denotes a point inside an even trixel. Y denotes the midpoint of this pixel, where B gets mapped (left). Points on the edgesindicated by broken blue lines are mapped to the corresponding even triangle, while the points of the solid red edge are mapped to the corresponding odd trixel. The left corner of even triangle (the corner of the two broken lines) is mapped to the even triangle itself (right).

points of a trixel, and finally, the midpoints of the sides of a trixel. We have considered these rotation centers, since they are exactly those points of the grid for which there are some special nonzero angles such that the rotation maps the triangular grid to itself.

Definition 2.15: (Digitized cell of the hexagonal grid) The digitized cell for the hexagonal grid is the region defined by the inequalities in the following way: Let $D_{\mathscr{H}}$ denote the digitized cell for the hexagonal grid. Then $D_{\mathscr{H}} = \{y \leq \sqrt{3}x + 2n\} \cap \{y > \sqrt{3}x + (2n-4)\} \cap \{y \geq -\sqrt{3}x + (2m-4)\} \cap \{y < -\sqrt{3}x + 2m\} \cap \{y < k\} \cap \{y \geq k-2\}$, for $n, m, k \in \mathbb{Z}$. Figure 2.5 shows the digitized cells for the square and the hexagonal grids.

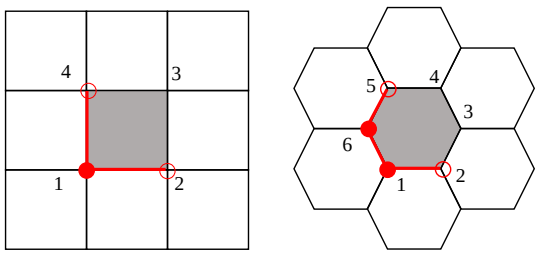

Figure 2.5: Digitized cells for the square grid (left) and the hexagonal grid (right), with the numbers assigned to corners. Digitized cell consists of the shaded main pixel, together with the edges and the vertices shown in bold red color.

Chapter 3

BIJECTIVITY OF THE NEIGHBORHOOD MOTION MAPS

Definition 3.1: Considering the digitized rotation of $\mathcal{T}_i$ $(i \in m, c, e)$ if 2 and/or 0 trixel centers lie in the same trixel after the specified digitized rotation, then we say that the digitized rotation is non-injective and/or non-surjective, respectively (see also figure 3.1).

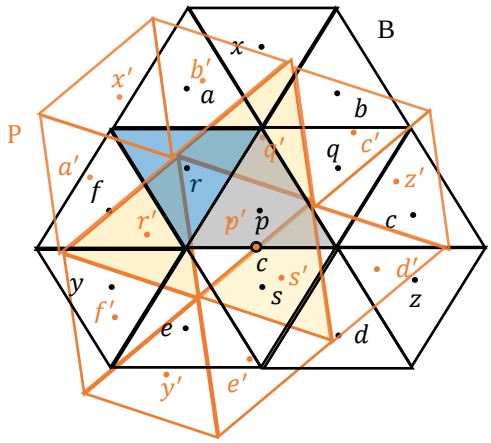

Figure 3.1: The grid part denoted by P is a part of the rotated form of the grid denoted by B.

In this thesis we are interested in rotations of a relatively small finite segment of the grid including a trixel and its twelve neighbors. According to Definition 3.1, we call a digitized rotation bijective if each of the 13 trixels are mapped to pairwise different trixels. To observe these local alterations of 12 neighborhood, we consider the neighborhood motion map concept on the grid defined as set of vectors, one for each neighbor showing the position of their images after the rotation. In figure 3.1,

p,q,r,s,a,b,c,d,e,f,x,y and z are the center points of the corresponding pixels before the rotation. The point p is the center of the main pixel and the other 12 points are the centers of the 12 neighbors, respectively. Point c is the rotation center and the rotation angle is 40° in positive direction (anti-clockwise). The $p',q',r',s',a',b',c',d',e',f',x',y'$ and z' are the rotated images of the p,q,r,s,a,b,c,d,e,f,x,y and z, respectively. As one can observe this digitized rotation is non-bijective. The images of the points p and q lie in the same, in fact the main, pixel. Further in this chapter, the center of the rotation is addressed by the coordinates $(0,0)^t$, bijectivity and non-bijectivity of the rotations will be proven by computing the image points.

For each case, even and odd orientations of the original main trixels are analyzed separately. This section is organized in the following way, in Subsection 3.1 we consider the digitized rotations of 12-neighborhood when the rotation center is a corner point of the main pixel. Similarly, in Subsections 3.2 and 3.3 , rotation with centers as the mid-point and the edge mid-points of the main pixel are considered, respectively.

3.1 Rotations around a Corner of a Trixel

The grid is mapped to itself by the angle of rotation $\theta \in \{n \cdot 60^\circ : n \in \mathbb{Z}\}$ when the center of rotation is a corner point. In this section the coordinate system $\mathscr{T}_c$ is used.

Proposition 3.1: If the center of the rotation is the left corner of an even pixel, then by considering the 12-neighborhood, the digitized rigid motions are given in Figure 3.2. The changes for the neighborhood motion maps occur at the following angles.

1. $\alpha_1 = \sin^{-1}\left(\frac{0.5}{\sqrt{7}}\right)$

2. $\alpha_2 = \cos^{-1}\left(\frac{3\sqrt{3}-\sqrt{19}}{4\sqrt{7}}\right) - \sin^{-1}\left(\frac{0.5}{\sqrt{7}}\right) - 60^\circ$
3. $\alpha_3 = \sin^{-1}(0.75) - 30^\circ$
4. $\alpha_4 = \cos^{-1}\left(\frac{\sqrt{19}}{2\sqrt{7}}\right) - \sin^{-1}\left(\frac{0.5}{\sqrt{7}}\right)$
5. $\alpha_5 = 30^\circ$
6. $\alpha_6 = \cos^{-1}\left(\frac{3\sqrt{3}+\sqrt{19}}{4\sqrt{7}}\right) - \sin^{-1}\left(\frac{0.5}{\sqrt{7}}\right)$
7. $\alpha_7 = \cos^{-1}(0.75)$
8. $\alpha_8 = \cos^{-1}\left(\frac{\sqrt{19}-3\sqrt{3}}{4\sqrt{7}}\right) - \sin^{-1}\left(\frac{2}{\sqrt{7}}\right)$
9. $\alpha_9 = 60^\circ - \sin^{-1}\left(\frac{0.5}{\sqrt{7}}\right)$
10. $\alpha_{10} = 60^\circ$
11. $k \cdot 60^\circ + \alpha_i$ where $i = \{1, ..., 10\}$ and $k = \{1, ..., 5\}$

Their approximated values are shown in figure 3.2.

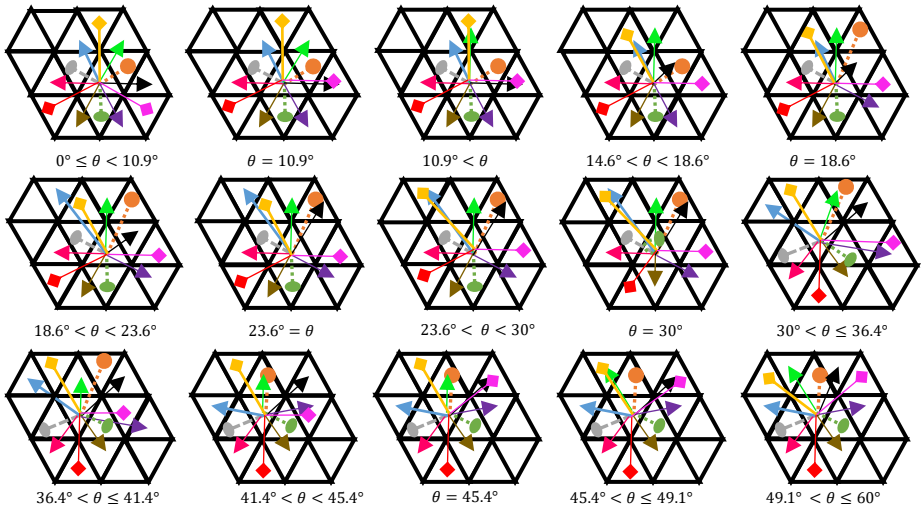

Figure 3.2: Neighborhood motion maps after rotation by the specified approximation angles

Proof. The angles are calculated by using polar coordinates, where $x = r\cos\omega$ and $y = r\sin\omega$. In figure 3.3, the point c is the rotation center. The points p and p' are the neighbor pixel center and its image after the rotation, respectively. The angle α

denotes the angle between the solid arrow (which connects the point p' to the origin) and the positive x-axis, and the angle $\theta = \alpha - 30°$. The angle α is calculated in the following way: $y = 1.5$ units and the radius (the length of both of the arrows cp and cp') is 2 units. Angle θ is computed as shown in Figure 3.3.

$$1.5 = 2\sin\alpha \Rightarrow \alpha = \sin^{-1}(0.75)$$
$$\theta = \sin^{-1}(0.75) - 30° \,(\approx 18.6°)\,,$$

where $30°$ is the angle between the $x-axis$ and the dotted arrow, which connects the point p to the origin c. The other angles are computed in a similar manner. □

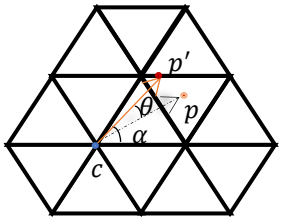

Figure 3.3: Center of the rotation (blue point, c), neighbor pixel center point (light pink, p), rotated image

Proposition 3.2: If the center of the rotation is the left corner of an even trixel, then the digitized rigid motion is injective if and only if $0 \leq \theta < \alpha_1 = \sin^{-1}\left(\frac{0.5}{\sqrt{7}}\right) \approx 10.9°$,or $\alpha_3 = \sin^{-1}(0.75) - 30° \approx 18.6° < \theta < \alpha_4 = \cos^{-1}\left(\frac{\sqrt{19}}{2\sqrt{7}}\right) - \sin^{-1}\left(\frac{0.5}{\sqrt{7}}\right) \approx 23.6°$ or $\alpha_6 = \cos^{-1}\left(\frac{3\sqrt{3}+\sqrt{19}}{4\sqrt{7}}\right) - \sin^{-1}\left(\frac{0.5}{\sqrt{7}}\right) \approx 36.4° < \theta \leq \alpha_7 = \cos^{-1}(0.75) \approx 41.4°$ or $\alpha_9 = 60° - \sin^{-1}\left(\frac{0.5}{\sqrt{7}}\right) \approx 49.1° < \theta < 60° + \alpha_1$ or $k \cdot 60° + \alpha_3 < \theta < k \cdot 60° + \alpha_4$ or $k \cdot 60° + \alpha_6 < \theta \leq k \cdot 60° + \alpha_7$ or $k \cdot 60° + \alpha_9 < \theta < k \cdot 60° + (60° + \alpha_1)$ where $k = \{1, ..., 5\}$.

Proof. Based on Proposition 3.1 (figure 3.2) the only injective maps are at $0 \leq \theta < \alpha_1 = \sin^{-1}\left(\frac{0.5}{\sqrt{7}}\right) \approx 10.9°$, or $\alpha_3 = \sin^{-1}(0.75) - 30° \approx 18.6° < \theta < \alpha_4 = \cos^{-1}\left(\frac{\sqrt{19}}{2\sqrt{7}}\right) - \sin^{-1}\left(\frac{0.5}{\sqrt{7}}\right) \approx 23.6°$

or $\alpha_6 = \cos^{-1}\left(\frac{3\sqrt{3}+\sqrt{19}}{4\sqrt{7}}\right) - \sin^{-1}\left(\frac{0.5}{\sqrt{7}}\right) \approx 36.4^\circ < \theta \leq \alpha_7 = \cos^{-1}(0.75) \approx$ 41.4° or $\alpha_9 = 60^\circ - \sin^{-1}\left(\frac{0.5}{\sqrt{7}}\right) \approx 49.1^\circ < \theta \leq 60^\circ$ □

For example, figure 3.4 shows the non-injective case of the rotation by showing a trixel to which two different trixels are mapped after the rotation. Point c is the center of the rotation with angle 30°. The points p and q are the centers of the main pixel and one of its neighbors and the points p' and q' are the rotated images of them, respectively. By our digitized cell concept, the points p' and q' belong to the same trixel since p' is on the anti-diagonal and q' is on the horizontal line. Now we consider other corners of the main pixel as rotation centers and/or also odd main pixels.

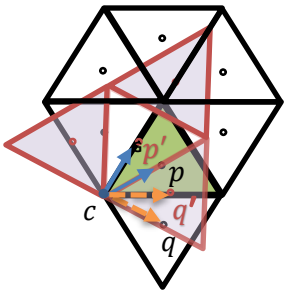

Figure 3.4: Solid arrows show how the center point p of the green trixel moves to p' and broken arrows show how the center q moves to q'. Both image points belong to the green trixel (G).

Remark 3.1: At every 60 degree turn, the center of the rotation is changed to another corner and the digitized rigid motions for this center can be observed from Proposition 3.1, figure 3.2. Figure 3.5 shows the changes of rotation centers with respect to the angles $0^\circ, 60^\circ, 120^\circ, 180^\circ, 240^\circ$ and 300°.

Remark 3.2: The images with respect to different corner positions of the center of the rotation can be observed by the rotated images of figure 3.2 in the same order. Instead of the formal description of the previous statements we give an example to show how

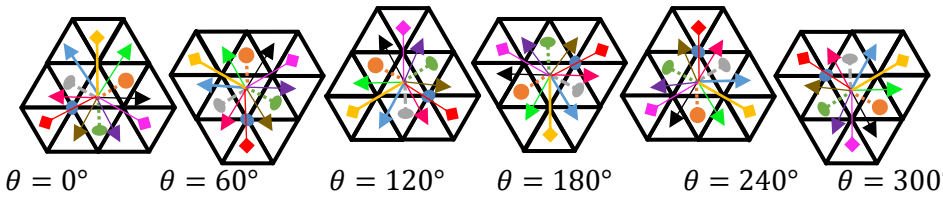

Figure 3.5: Changes of rotation center (blue corner) with respect to the angles.

they can be understood. The motion maps for rotations around the lower corner of an odd pixel can be observed directly from figure 3.2. Figure 3.6 shows the first 2 images of this rotation by the specified approximation angles. The first image is exactly 60° rotated form of the first image of figure 3.2. The order of the images and angles of the digitized rotations from the lower corner of an odd pixel follows the order of figure 3.2.

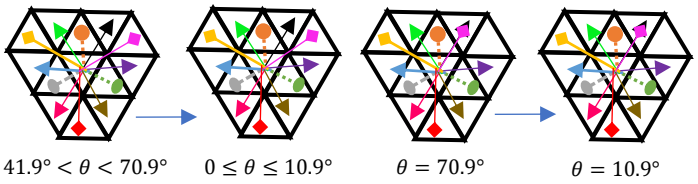

Figure 3.6: The first image of rotation around the lower corner of the odd pixel (2 images on the left), the second image of rotation around the lower corner of the odd pixel (2 images on the right).

The images and the angles of all rotations around any corner point can be obtained in a similar way:

- 0 degree is the starting point of rotation around the left corner of the even pixel (Proposition 3.1, figure 3.2).
- The first image of rotation around the bottom corner of the odd pixel is 60° rotated form of the images of figure 3.2 in the same order as figure 3.2.
- The first image of rotation around the right corner of the even pixel is 120° rotated form of the images of figure 3.2 in the same order as figure 3.2.
- The first image of rotation around the right corner of the odd pixel is 180° rotated

form of the images of figure 3.2 in the same order as figure 3.2.

- The first image of rotation around the upper corner of the even pixel is 240° rotated form of the images of figure 3.2 in the same order as figure 3.2.
- The first image of rotation around the left corner of the odd pixel is 300° rotated form of the images of figure 3.2 in the same order as figure 3.2.

Proposition 3.3: If the center of the rotation is the corner point of a given trixel, then the changes of the neighborhood motion maps for two distinct neighbor points occur at the same angle (with respect to the definition of the digitized cell) if and only if the neighbors are equidistant from the center of the rotation with $k \cdot \frac{\pi}{3}$ degrees (where $k = 1, 2, 3$) in between them (considering the angle at the rotation center in the triangle formed by this point and the center of the corresponding neighbor trixels).

Proof. Angle computations in Proposition 3.2 confirm the required results. For the reverse direction also note that, if two distinct neighbors are equidistant from the center of the rotation, after rotation by specified angles the grid gets mapped to itself, and hence the neighbors will get mapped to one another. □

We show some examples in figure 3.7.

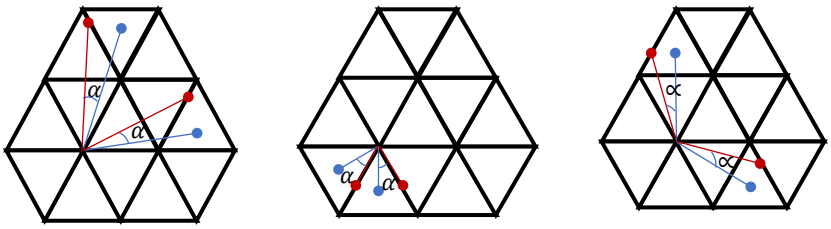

Figure 3.7: Digitized rotations with rotation center the corner point.

3.2 Rotations Around the Center of a Trixel

The grid is mapped to itself by the angle of rotation $\theta \in \{n \cdot 120^\circ : n \in \mathbb{Z}\}$ when the center of the rotation is the center of a trixel [19]. The proofs of the coming propositions are in similar nature to the proofs of the previous subsection, thus they are excluded.

Proposition 3.4: If the center of the rotation is the midpoint of an even pixel, then by considering the 12 neighborhood, the digitized rigid motions are given in figure 3.8. The changes of the motion map occur for the angles:

1. $\alpha_1 = 30^\circ - \sin^{-1}\left(\frac{1}{4}\right)$
2. $\alpha_2 = \cos^{-1}\left(\frac{-\sqrt{3}+\sqrt{11}}{4\sqrt{3}}\right) - 60^\circ$
3. $\alpha_3 = 60^\circ - \sin^{-1}\left(\frac{1}{\sqrt{3}}\right)$
4. $\alpha_4 = \sin^{-1}\left(\frac{1}{\sqrt{3}}\right)$
5. $\alpha_5 = 60^\circ + \sin^{-1}\left(\frac{-1}{2\sqrt{3}}\right)$
6. $\alpha_6 = 60^\circ$
7. $\alpha_7 = \cos^{-1}\left(\frac{-\sqrt{3}+\sqrt{11}}{4\sqrt{3}}\right)$
8. $\alpha_8 = 120^\circ - \sin^{-1}\left(\frac{1}{\sqrt{3}}\right)$
9. $\alpha_9 = 60^\circ + \sin^{-1}\left(\frac{1}{\sqrt{3}}\right)$
10. $\alpha_{10} = 120^\circ + \sin^{-1}\left(\frac{-1}{2\sqrt{3}}\right)$
11. $\alpha_{11} = \sin^{-1}\left(\frac{1}{4}\right)$
12. $k \cdot 120^\circ + \alpha_i$ where $i = \{1, ..., 11\}$ and $k = \{1, 2\}$

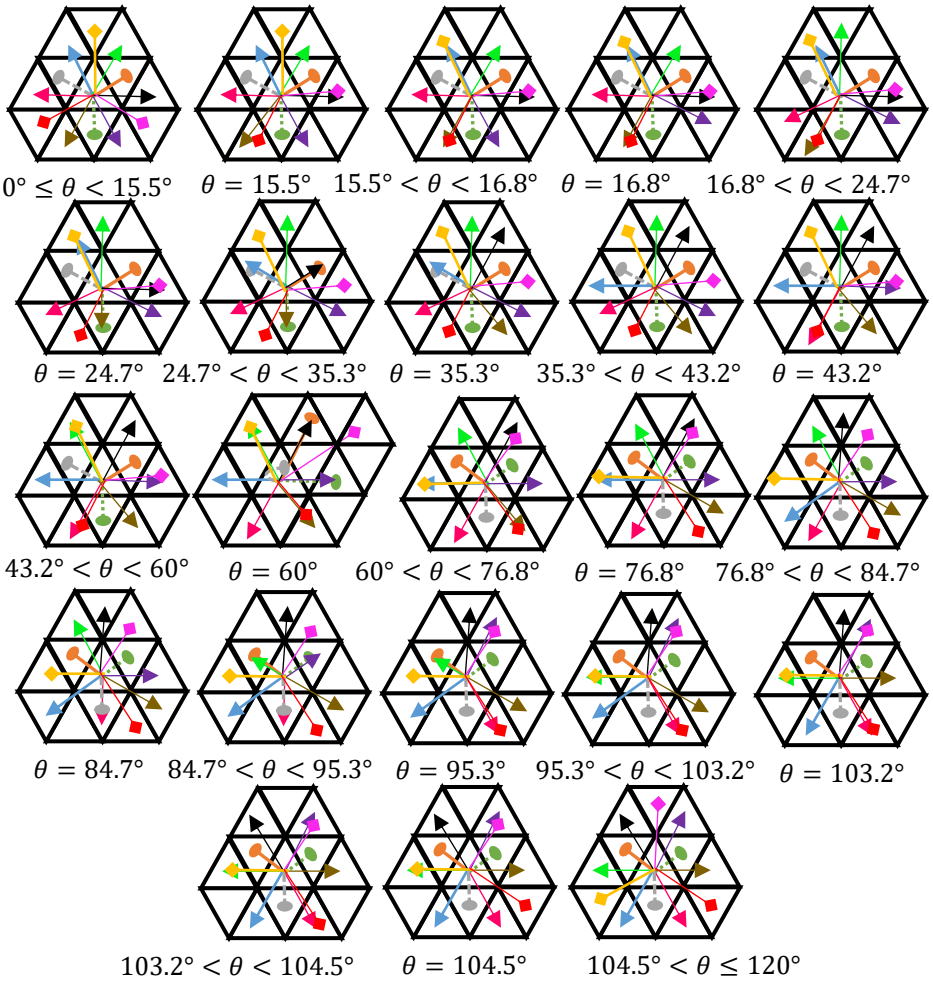

Figure 3.8: Neighborhood motion maps after rotation around the midpoint of the even trixel by the specified angles.

Proposition 3.5: If the center of the rotation is the midpoint of an even pixel, then the digitized rigid motion is injective if and only if $0° \leq \theta < \alpha_1 = 30° - \sin^{-1}\left(\frac{1}{4}\right) \approx 15.5°$, or $\alpha_4 = \sin^{-1}\left(\frac{1}{\sqrt{3}}\right) \approx 35.3° < \theta < \alpha_5 = 60° + \sin^{-1}\left(\frac{-1}{2\sqrt{3}}\right) \approx 43.2°$, or $\alpha_7 = \cos^{-1}\left(\frac{-\sqrt{3}+\sqrt{11}}{4\sqrt{3}}\right) \approx 76.8° < \theta < \alpha_8 = 120° - \sin^{-1}\left(\frac{1}{\sqrt{3}}\right) \approx 84.7°$, or $\alpha_{11} = \sin^{-1}\left(\frac{1}{4}\right) \approx 104.5° < \theta < 120° + \alpha_1$, or $k \cdot 120° + \alpha_4 < \theta < k \cdot 120° + \alpha_5$, or $k \cdot 120° + \alpha_7 < \theta < k \cdot 120° + \alpha_8$, or $k \cdot 120° + \alpha_{11} < \theta < k \cdot 120° + (120° + \alpha_1)$ where $k = \{1, 2\}$.

Proposition 3.6: If the center of the rotation is the midpoint of an odd pixel, then the changes for the neighborhood motion maps occur at the same angles as the rotation with center the midpoint of an even pixel. The digitized rigid motions are given in figure 3.9.

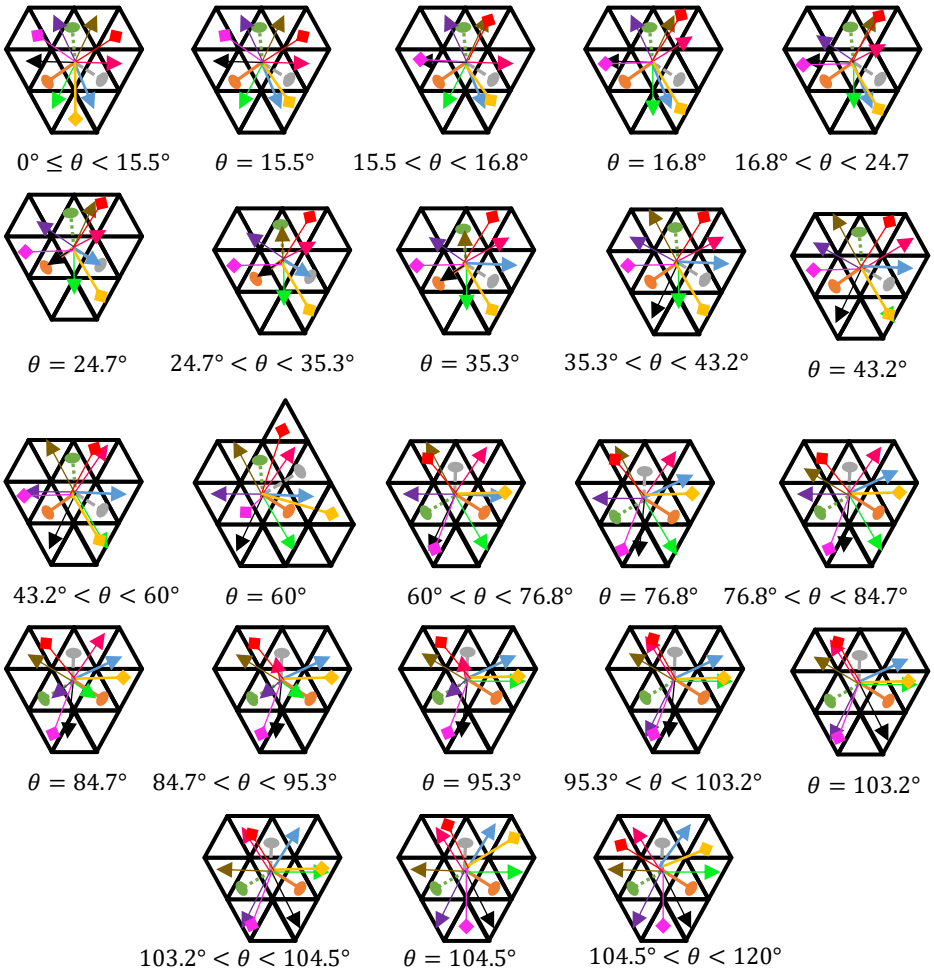

Figure 3.9: Neighborhood motion maps after rotation around the midpoint of an odd pixel by the specified angles.

Proposition 3.7: If the center of the rotation is the midpoint of a given trixel, then the changes of the neighborhood motion maps for two distinct neighbor points (with respect to the definition of digitized cell) occur at the same angle

i. For the 1-neighbors

ii. For the strict 3-neighbors,

iii. If and only if the strict 2-neighbors have $2 \cdot \frac{\pi}{3}$ degrees between them

We show some cases in figure 3.10.

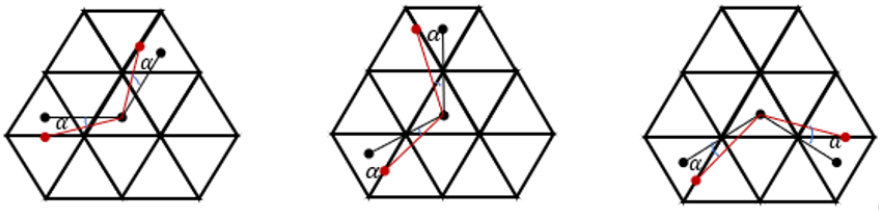

Figure 3.10: Digitized rotations with rotation center the midpoint of the trixel.

3.3 Rotations Around the Midpoint of an Edge

The grid is mapped to itself by the angle of rotation $\theta \in \{n \cdot 180^\circ : n \in \mathbb{Z}\}$ when the center of the rotation is the midpoint of an edge [19,20].

Proposition 3.8: If the center of the rotation is the midpoint of the lower edge of an even trixel, then by considering 12-neighborhood, the digitized rigid motions are given in figure 3.11 and 3.12. The changes of the motion maps occur for the angles α_1 to α_{49}:

1. $\alpha_1 = 90^\circ - \cos^{-1}\left(\frac{6\sqrt{3}-2\sqrt{91}}{8\sqrt{5}}\right)$
2. $\alpha_2 = \cos^{-1}\left(\frac{-6\sqrt{3}-2\sqrt{67}}{8\sqrt{19}}\right) - \sin^{-1}\left(\sqrt{\frac{16}{19}}\right)$
3. $\alpha_3 = \sin^{-1}\left(\frac{1}{\sqrt{13}}\right)$
4. $\alpha_4 = \cos^{-1}\left(\frac{6\sqrt{3}+2\sqrt{43}}{8\sqrt{13}}\right) - \sin^{-1}\left(\frac{1}{\sqrt{13}}\right)$
5. $\alpha_5 = \sin^{-1}\left(\frac{4}{\sqrt{19}}\right) - \sin^{-1}\left(\frac{3}{\sqrt{19}}\right)$
6. $\alpha_6 = \sin^{-1}\left(\frac{2}{\sqrt{7}}\right) - \cos^{-1}\left(\frac{6\sqrt{3}+2\sqrt{91}}{8\sqrt{7}}\right)$

7. $\alpha_7 = \cos^{-1}\left(\frac{-6\sqrt{3}-2\sqrt{67}}{8\sqrt{19}}\right) - \left(180^\circ - \sin^{-1}\left(\sqrt{\frac{16}{19}}\right)\right)$
8. $\alpha_8 = \cos^{-1}\left(\frac{6\sqrt{3}-2\sqrt{67}}{8\sqrt{19}}\right) - \sin^{-1}\left(\frac{4}{\sqrt{19}}\right)$
9. $\alpha_9 = 90^\circ - \cos^{-1}\left(\frac{-18\sqrt{3}+2\sqrt{91}}{8\sqrt{5}}\right)$
10. $\alpha_{10} = 180^\circ - \cos^{-1}\left(\frac{-6\sqrt{3}+2\sqrt{91}}{8\sqrt{7}}\right) - \sin^{-1}\left(\frac{-2}{\sqrt{7}}\right)$
11. $\alpha_{11} = \sin^{-1}\left(\sqrt{\frac{9}{13}}\right) - \sin^{-1}\left(\sqrt{\frac{1}{13}}\right)$
12. $\alpha_{12} = 180^\circ - \cos^{-1}\left(\frac{6\sqrt{3}-2\sqrt{91}}{8\sqrt{7}}\right) - \sin^{-1}\left(\frac{-2}{\sqrt{7}}\right)$
13. $\alpha_{13} = 90^\circ - \cos^{-1}\left(\frac{-6\sqrt{3}-2\sqrt{91}}{8\sqrt{5}}\right)$
14. $\alpha_{14} = \sin^{-1}\left(\frac{2}{\sqrt{7}}\right)$
15. $\alpha_{15} = 180^\circ - \cos^{-1}\left(\frac{-6\sqrt{3}-2\sqrt{43}}{8\sqrt{13}}\right) - \sin^{-1}\left(\frac{1}{\sqrt{13}}\right)$
16. $\alpha_{16} = 90^\circ - \sin^{-1}\left(\frac{1.5}{2.5}\right)$
17. $\alpha_{17} = \sin^{-1}\left(\frac{4}{\sqrt{19}}\right)$
18. $\alpha_{18} = \cos^{-1}\left(\frac{-6\sqrt{3}+2\sqrt{43}}{8\sqrt{13}}\right) - \sin^{-1}\left(\frac{1}{\sqrt{13}}\right)$
19. $\alpha_{19} = 180^\circ - \sin^{-1}\left(\sqrt{\frac{9}{19}}\right) - \sin^{-1}\left(\sqrt{\frac{16}{19}}\right)$
20. $\alpha_{20} = \sin^{-1}\left(\sqrt{\frac{9}{13}}\right) + \sin^{-1}\left(\sqrt{\frac{1}{13}}\right)$
21. $\alpha_{21} = \cos^{-1}\left(\frac{-6\sqrt{3}-2\sqrt{67}}{8\sqrt{19}}\right) - \sin^{-1}\left(\frac{4}{\sqrt{19}}\right)$
22. $\alpha_{22} = \cos^{-1}\left(\frac{6\sqrt{3}+2\sqrt{19}}{8\sqrt{19}}\right) - \sin^{-1}\left(\frac{2}{\sqrt{7}}\right)$
23. $\alpha_{23} = \cos^{-1}\left(\frac{6\sqrt{3}-2\sqrt{43}}{8\sqrt{13}}\right) - \cos^{-1}\left(\sqrt{\frac{12}{13}}\right)$
24. $\alpha_{24} = 90^\circ - \cos^{-1}\left(\frac{18\sqrt{3}+2\sqrt{91}}{8\sqrt{5}}\right)$
25. $\alpha_{25} = 90^\circ$
26. $\alpha_{26} = 90^\circ + \cos^{-1}\left(\frac{18\sqrt{3}+2\sqrt{91}}{8\sqrt{5}}\right)$

27. $\alpha_{27} = 180^\circ - \cos^{-1}\left(\frac{6\sqrt{3}-2\sqrt{43}}{8\sqrt{13}}\right) + \cos^{-1}\left(\frac{2\sqrt{3}}{\sqrt{13}}\right)$
28. $\alpha_{28} = 180^\circ - \cos^{-1}\left(\frac{6\sqrt{3}+2\sqrt{19}}{8\sqrt{7}}\right) + \cos^{-1}\left(\frac{\sqrt{3}}{\sqrt{7}}\right)$
29. $\alpha_{29} = \cos^{-1}\left(\frac{-6\sqrt{3}-\sqrt{67}}{8\sqrt{19}}\right) + \cos^{-1}\left(\frac{\sqrt{3}}{\sqrt{19}}\right)$
30. $\alpha_{30} = 180^\circ - \sin^{-1}\left(\frac{3}{\sqrt{13}}\right) - \cos^{-1}\left(\frac{2\sqrt{3}}{\sqrt{13}}\right)$
31. $\alpha_{31} = \sin^{-1}\left(\frac{3}{\sqrt{19}}\right) - \cos^{-1}\left(\frac{\sqrt{3}}{\sqrt{19}}\right)$
32. $\alpha_{32} = 180^\circ - \cos^{-1}\left(\frac{-6\sqrt{3}+2\sqrt{43}}{8\sqrt{13}}\right) + \cos^{-1}\left(\frac{\sqrt{12}}{\sqrt{13}}\right)$
33. $\alpha_{33} = 180^\circ - \cos^{-1}\left(\frac{\sqrt{3}}{\sqrt{19}}\right)$
34. $\alpha_{34} = 90^\circ + \sin^{-1}\left(\frac{1.5}{2.5}\right)$
35. $\alpha_{35} = \cos^{-1}\left(\frac{-6\sqrt{3}-2\sqrt{43}}{8\sqrt{13}}\right) - \sin^{-1}\left(\frac{1}{\sqrt{13}}\right)$
36. $\alpha_{36} = 180^\circ - \sin^{-1}\left(\frac{2}{\sqrt{7}}\right)$
37. $\alpha_{37} = 90^\circ + \cos^{-1}\left(\frac{-6\sqrt{3}-2\sqrt{91}}{8\sqrt{5}}\right)$
38. $\alpha_{38} = \cos^{-1}\left(\frac{6\sqrt{3}-2\sqrt{19}}{8\sqrt{7}}\right) + \sin^{-1}\left(\frac{2}{\sqrt{7}}\right)$
39. $\alpha_{39} = 180^\circ - \sin^{-1}\left(\frac{3}{\sqrt{13}}\right) + \sin^{-1}\left(\frac{1}{\sqrt{13}}\right)$
40. $\alpha_{40} = \cos^{-1}\left(\frac{-6\sqrt{3}-2\sqrt{19}}{8\sqrt{7}}\right) + \sin^{-1}\left(\frac{2}{\sqrt{7}}\right)$
41. $\alpha_{41} = 90^\circ + \cos^{-1}\left(\frac{-18\sqrt{3}+2\sqrt{19}}{8\sqrt{5}}\right)$
42. $\alpha_{42} = 180^\circ - \cos^{-1}\left(\frac{6\sqrt{3}-2\sqrt{67}}{8\sqrt{19}}\right) + \sin^{-1}\left(\frac{4}{\sqrt{19}}\right)$
43. $\alpha_{43} = 360^\circ - \cos^{-1}\left(\frac{-6\sqrt{3}-2\sqrt{67}}{8\sqrt{19}}\right) - \sin^{-1}\left(\frac{4}{\sqrt{19}}\right)$
44. $\alpha_{44} = 180^\circ + \cos^{-1}\left(\frac{6\sqrt{3}+2\sqrt{19}}{8\sqrt{7}}\right) - \sin^{-1}\left(\frac{2}{\sqrt{7}}\right)$
45. $\alpha_{45} = 180^\circ + \sin^{-1}\left(\frac{3}{\sqrt{19}}\right) - \sin^{-1}\left(\frac{4}{\sqrt{19}}\right)$

46. $\alpha_{46} = 180^\circ - \cos^{-1}\left(\frac{6\sqrt{3}+2\sqrt{43}}{8\sqrt{13}}\right) - \sin^{-1}\left(\frac{1}{\sqrt{13}}\right)$
47. $\alpha_{47} = 180^\circ - \sin^{-1}\left(\frac{1}{\sqrt{13}}\right)$
48. $\alpha_{48} = 180^\circ - \cos^{-1}\left(\frac{-6\sqrt{3}+2\sqrt{67}}{8\sqrt{19}}\right) + \sin^{-1}\left(\frac{4}{\sqrt{19}}\right)$
49. $\alpha_{48} = 90^\circ + \cos^{-1}\left(\frac{6\sqrt{3}-2\sqrt{43}}{8\sqrt{5}}\right)$
50. $180^\circ + \alpha_i, i = \{1, ..., 49\}$

Their approximate values are shown in figures 3.11, 3.12 and 3.13.

Proof. We consider the coordinate system $\mathscr{T}_e$. The angles are calculated by using polar coordinates, where $x = r\cos\omega$ and $y = r\sin\omega$. Figure 3.14 shows that the point c is the midpoint of the bottom edge of the main pixel, which is the rotation center as well. Point p is the center of one of the neighbor trixels. The line L, is the line that passes through the right edge of the main pixel. Further, the circle C, is the circle whose radius is equal to the distance between c and p. The angles α and β denote the angles between the horizontal line (holding the point c) and the arrows which connect the points p and p' to the center of the rotation, c, respectively. The equation of the line L is $y = -\sqrt{3}x + 1.5$ and the equation of the circle C is $x^2 + y^2 = \frac{7}{4}$. The point p' is the intersection point of L and C , the x coordinate of this point is $\frac{3\sqrt{3}-\sqrt{19}}{8}$. Since $x = r\cos\beta$ and $r = \frac{\sqrt{7}}{2}$, then $\beta = \cos^{-1}\left(\frac{6\sqrt{3}-2\sqrt{19}}{8\sqrt{7}}\right)$, thus the angle of rotation is equal to $\cos^{-1}\left(\frac{6\sqrt{3}-2\sqrt{19}}{8\sqrt{7}}\right) - \cos^{-1}\left(\frac{\sqrt{3}}{\sqrt{7}}\right)$ where $\cos^{-1}\left(\frac{\sqrt{3}}{\sqrt{7}}\right) = \alpha$. Other angles are computed similarly. □

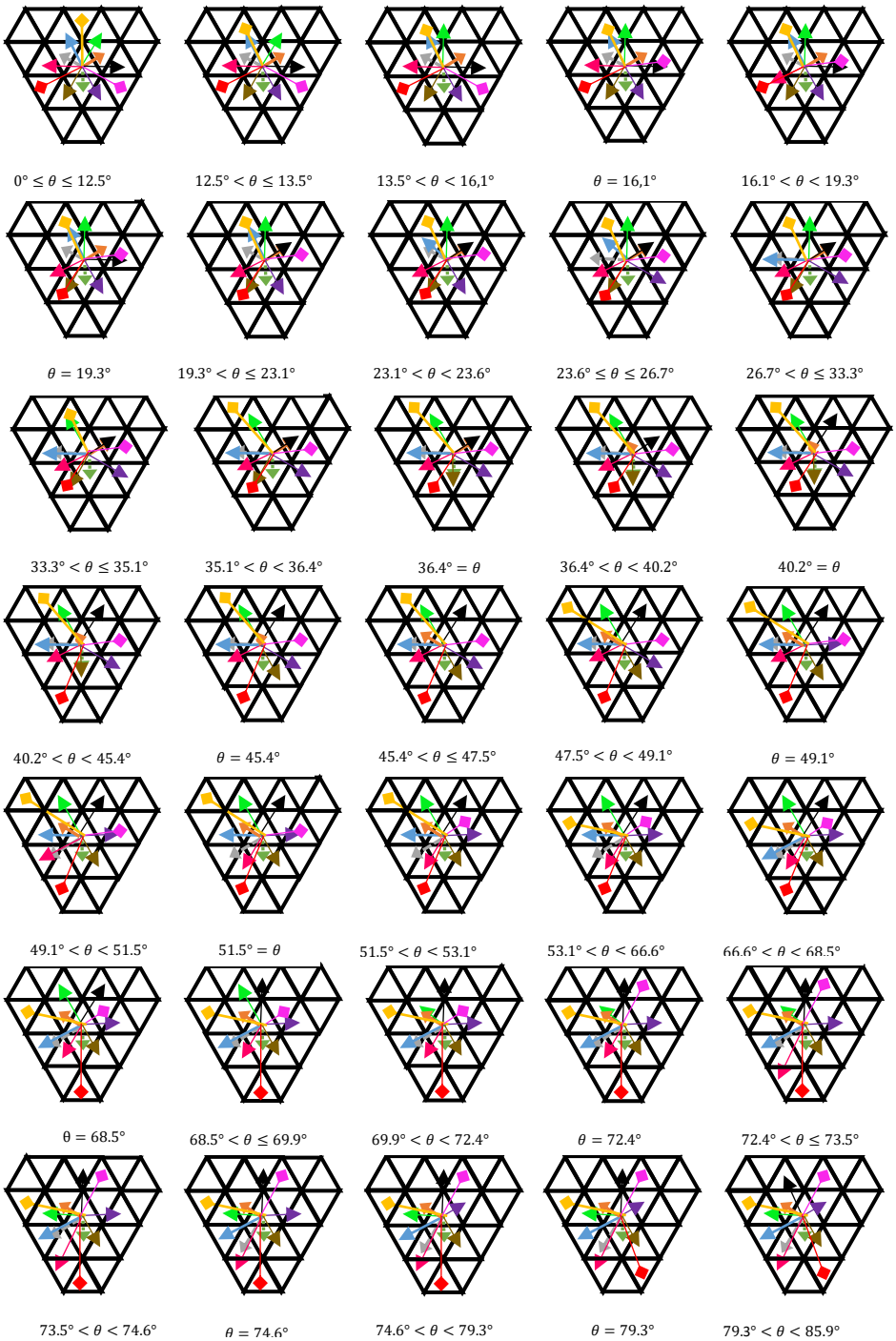

Figure 3.11: Neighborhood motion maps for rotation around lower edge midpoint

Proposition 3.9: If the center of the rotation is the midpoint of the lower edge of an even pixel, then the digitized rigid motion is injective if and only if $0° \leq \theta < \alpha_1 \approx 12.5°$ or $51.5° \approx \alpha_{15} < \theta \leq \alpha_{17} \approx 66.6°$ or $74.6° \approx \alpha_{22} \leq \theta < \alpha_{24} \approx 85.9°$ or $94.2° \approx \alpha_{26} < \theta \leq \alpha_{28} \approx 105.4°$ or $113.4° \approx \alpha_{33} < \theta \leq \alpha_{35} \approx 128.5°$ or $174.6° \approx \alpha_{49} \leq$

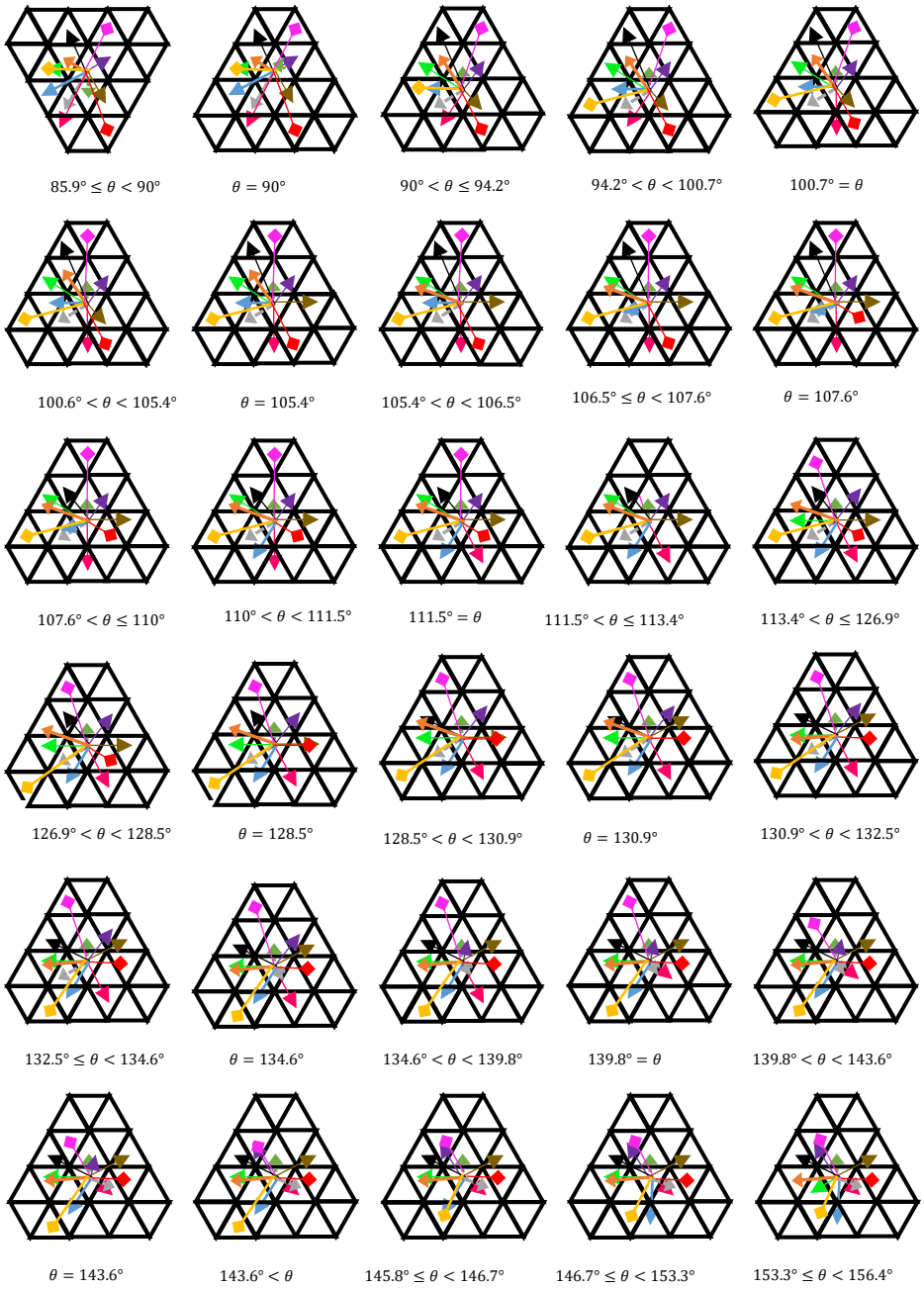

Figure 3.12: Neighborhood motion maps for rotation around lower edge midpoint

$\theta \leq 180^\circ + \alpha_1$ or $180^\circ + \alpha_{15} \leq \theta \leq 180^\circ + \alpha_{17}$ or $180^\circ + \alpha_{22} \leq \theta \leq 180^\circ + \alpha_{24}$ or $180^\circ + \alpha_{26} \leq \theta \leq 180^\circ + \alpha_{28}$ or $180^\circ + \alpha_{33} \leq \theta \leq 180^\circ + \alpha_{35}$ or $180^\circ + \alpha_{49} \leq \theta \leq 360^\circ$

.

Proposition 3.10: Digitized rigid motion maps for rotation center at the other edge

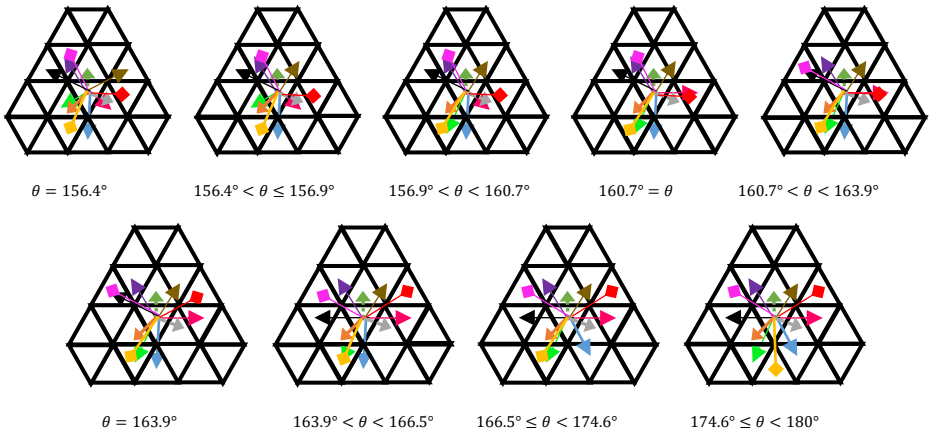

Figure 3.13: Neighborhood motion maps for rotation around lower edge midpoint.

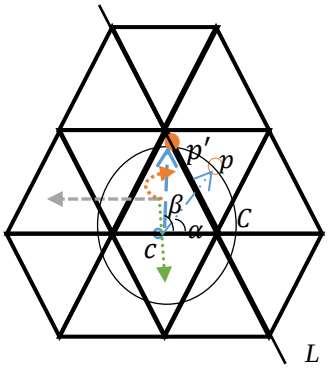

Figure 3.14: Blue point c indicates the center of the rotation where the orange point p and p' indicate the center of the right neighbor pixel and its image after rotation, respectively.

midpoints are obtained from figures 3.11, 3.12 and 3.13 as described below.

- The first 3 neighborhood motion maps of rotations centered at the left edge midpoint of an even triangle is shown in figure 3.15. (240 degree rotated forms of figures 3.11,3.12 and 3.13.)

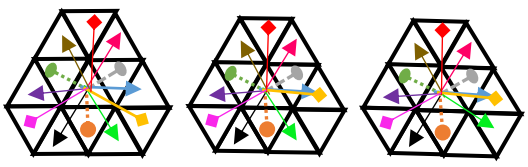

Figure 3.15: The first 3 neighborhood motion maps of rotations centered at the left edge midpoint of an even triangle with 12-neighbors.

- The first 3 neighborhood motion maps of rotations centered at the right edge midpoint of an even triangle is shown in figure 3.16. (120 degree rotated forms of the images of figures 3.11,3.12 and 3.13.)

Figure 3.16: The first 3 neighborhood motion maps of rotations centered at the right edge midpoint of an even triangle with 12-neighbors.

Remark 3.3: The images of figure 3.17 (for rotation center at the midpoints of an edge of an odd main trixel) can be observed by 180 degree rotated form of the Figures with the even main trixels. Figure shows that, the bottom edge midpoint of an even pixel is mapped to the upper edge midpoint of an odd pixel at 180° (first and second subfigures), right edge midpoint of an even pixel is mapped to the left edge midpoint of an odd pixel at 180° (third and fourth subfigures) and left edge midpoint of an even pixel is mapped to the right edge midpoint of an odd pixel at 180° (fifth and sixth subfigures.)

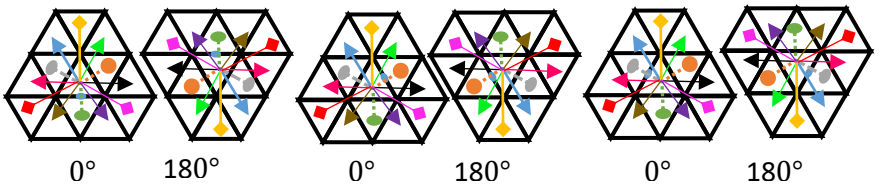

Figure 3.17: Rotations around edge mid-points.

Proposition 3.11: If the center of the rotation is the midpoint of an edge, then the changes of the neighborhood motion maps for two distinct neighbor points occur at the same angle (with respect to the definition of digitized cell) if and only if the neighbors are equidistant from the center and these three points lie on the same line. We show some cases in figure 3.18.

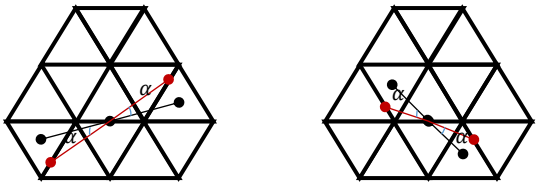

Figure 3.18: Digitized rotations with rotation center the midpoint of an edge.

Chapter 4

COMPARISON OF THE THREE REGULAR GRIDS

In this section, considering only the closest neighbors, we will compare the results for the bijectivity of the digitized rotations of the three grids. The non-injectivity is important as this notion determines the information loss in the image. In our experiment, for all three grids, we consider digitized rotations (with respect to different rotation centers) for each integer angle between 0 and 360 degrees [37]. We give a short theoretical explanation about how these results are achieved. With respect to the corresponding center of rotation, first, the coordinates of the main pixel with its closest neighbors are computed (see section 2). The rotation matrix of the plane then produces the rotated coordinates. For the square grid, section 2.2 gives the rounding formulas for the digitized coordinates. In the case of the hexagonal grid, triplet coordinates are assigned to the closest neighbors after the digitized rotation. After rotating the closest neighbors with the Cartesian coordinates, we use the definition of the hexagonal digitized cell (again given in section 2.2) to produce these triplet coordinates. For the hexagonal and the triangular grids, it is much simpler to view injectivity/ non-injectivity after the digitized rotation when the triplet coordinates are used, therefore we have this approach. Finally for the triangular grid, again, triplet coordinates are assigned to the closest neighbors after the digitized rotation, by using the definition of the digitized cell of the triangular grid. A more theoretical approach for the triangular grid can be found in our earlier conference paper [42], which we shall explain here.

Let (x', y') denote the Cartesian coordinates of the image point after rotation by θ degrees. The conversion, then, to the triplet coordinates, by taking into account the digitization operator, is described below: Let L be the line $y = mx$ where $m \neq 0$, and let the transformation T be the orthogonal projection on the line L. Then the expression for T is given by

$$T(x,y) = \left(\frac{x+ym}{m^2+1}, \frac{xm+ym^2}{m^2+1} \right)$$

Note that the i-axis and the k-axis have the equations $y = \frac{1}{\sqrt{3}}x$ and $y = -\frac{1}{\sqrt{3}}x$, respectively, on the triangular plane. In this way one can obtain the orthogonal projections on these two coordinate axes. Below we provide formulas to obtain the corresponding (i, j, k) triplet, with the digitization also taken into consideration. Note that if the origin O is taken to be the center of a certain starting trixel where all three coordinate axes i, j and k meet, then the diagonal and the anti-diagonal grid lines have the equations $y = -\sqrt{3}x + C$ and, $y = \sqrt{3}x + C$, respectively, where $C = 3m + 1$ with $m \in \mathbb{Z}$. We show next how to obtain the (i, j, k) triplet after the digitized rotation, by using the floor and the ceiling functions.

1. The coordinate i:

   If $y' > -\sqrt{3}x'$, then $i = \left\lfloor \frac{\sqrt{x'^2+y'^2}+1}{1.5} \right\rfloor$

   and

   if $y' < -\sqrt{3}x'$, then $i = \left\lfloor -\frac{\sqrt{x'^2+y'^2}+1}{1.5} \right\rfloor$.

   If $y' = -\sqrt{3}x'$, then $i = 0$.

2. The coordinate $j = \left\lceil \frac{-y'-0.5}{1.5} \right\rceil$

3. The coordinate k

   If $y' > \sqrt{3}x'$, then $k = \left\lceil \frac{\sqrt{x'^2+y'^2}-0.5}{1.5} \right\rceil$

   and

   if $y' < \sqrt{3}x'$, then $k = \left\lceil -\frac{\sqrt{x'^2+y'^2}-0.5}{1.5} \right\rceil$.

If $y' = \sqrt{3}x'$, then $k = 0$.

In each subsection below, digitized rotations around the center, gridpoint and the edge midpoint will be considered.

4.1 Rotations around Center of a Pixel

In square grid, the vectors of the main pixel with its neighbors are $(0,0)$, $(1,0)$, $(0,1)$, $(-1,0)$ and $(0,-1)$. The experiment shows that the digitized rotations are injective for every integer angle between 0 and 360 degrees in this case. In hexagonal grid, the coordinates of the main hexel and the neighbors are given by $(0,0)$, $(\sqrt{3},1)$, $(0,2)$, $(-\sqrt{3},1)$, $(-\sqrt{3},-1)$, $(0,-2)$ and $(\sqrt{3},-1)$. In this grid, we have non-bijectivity at 6 different integer angles (at angles $30^\circ, 90^\circ, 150^\circ$, $210^\circ, 270^\circ$ and 330° to be more precise). For the triangular grid, if the main trixel is an even one, then the coordinates of the main trixel with its 1-neighbors are $(0,0)$, $(\frac{\sqrt{3}}{2},\frac{1}{2})$, $(-\frac{\sqrt{3}}{2},\frac{1}{2})$ and $(0,-1)$, whereas if the main trixel is an odd one, then coordinates are $(0,0)$, $(\frac{\sqrt{3}}{2},-\frac{1}{2})$, $(-\frac{\sqrt{3}}{2},-\frac{1}{2})$ and $(0,1)$. In triangular grid, if the center of the rotation is the midpoint of an even trixel, we have non-bijectivity at only 3 different integer angles (at $60^\circ, 180^\circ$ and 300°). However, if the center of the rotation is the midpoint of an odd trixel, then the digitized rotations are injective for all the integer angles, as it is in the case of the square grid. For the square grid pixel loss is none due to the injectivity whereas for both the hexagonal and the triangular grids pixel loss is always 1, in the case when bijectivity fails. In the hexagonal grid, in the view of non-bijectivity, 7 hexels are mapped to 6 hexels, meaning that 14.3 percent of the information of the image at the main pixel's neighborhood is lost. This percentage is a little higher, 25 percent, in the triangular grid since 4 trixels are mapped to 3 trixels. All the non-bijective digitized rotations in triangular and hexagonal grids produce the same images, respectively, therefore in figure 4.1 we show only one case for each of them. In the figure, begining

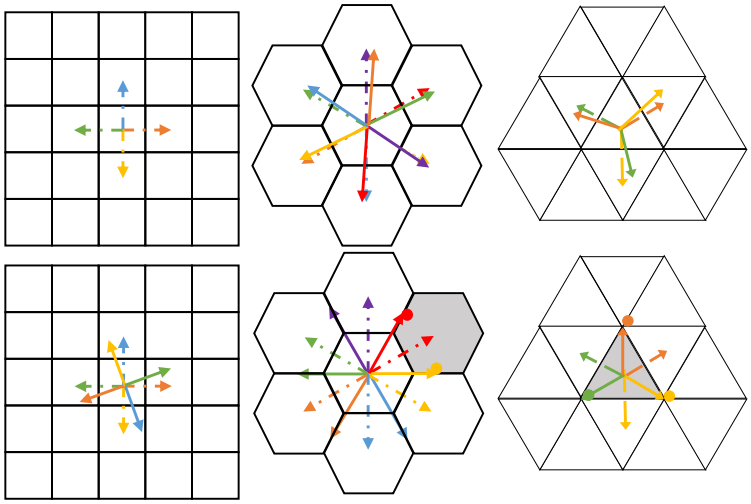

Figure 4.1: Digitized rotations of the main pixel with its closest neighbors on the 3 grids.

image and a bijective digitized rotation by 189 degrees on the square grid (first column). Bijective digitized rotation by 236° and a non-bijective one by 30° (second column) on the hexagonal grid. Finally a bijective digitized rotation by 131° and a non-bijective one by 60° (third column) on the triangular grid (the main trixel is mapped to itself). In the hexagonal and triangular grids, in other non-bijective cases, only the colors of the arrows are changing, producing the same images. Broken arrows denote the neighbors before the digitized rotation whereas solid ones denote the neighbors after the digitized rotation. Non-injective pixels, after the rotations, are shaded in grey color.

4.2 Rotations around a Gridpoint (Vertex of the Grid)

In this section we consider the rotation center at a gridpoint, i.e., crossing point of the gridlines. First, let us consider the bottom left corner of the main pixel, i.e. corner 1. The vectors of the main pixel with neighbors are given in the first rows of tables 4.1, 4.2, 4.3. In this case, square and the triangular grids both have non-bijectivity at 2 different integer angles (at 45° and 315° for the square grid, and at 30° and 330° for the triangular grid, having even main pixel). The pixel loss is 1 in both cases;

however for the square grid 20 percent of the information of the image around the main pixel's neighborhood is lost whereas for the triangular grid, this loss is 25 percent. The hexagonal grid, with non-injectivity at 36 different integer angles; for all integer angles θ in the intervals $20^\circ \leq \theta \leq 25^\circ$, $95^\circ \leq \theta \leq 100^\circ$, $140^\circ \leq \theta \leq 145^\circ$, $215^\circ \leq \theta \leq 220^\circ$, $260^\circ \leq \theta \leq 265^\circ$, and $335^\circ \leq \theta \leq 340^\circ$, gives the worst performance compared with the square or the triangular grid. The number of non-bijectivity cases are valid for rotation center taken at any given corner of the main pixel. For the triangular grid, at every multiple of 60 degrees the grid gets mapped onto itself, and the center of rotation is changed to another corner, so the images with respect to different corner positions are the same images, having the same order of appearance, with various starting images [43]. In square and hexagonal grids, when the center of rotation is a gridpoint, then grid gets mapped onto itself at every multiple of 90° and 120°, respectively. In case of the square grid, at every multiple of 90°, we will obtain a different corner of the main pixel so same images (in the same order) are obtained with different starting images. For example, in square grid, the image at 1° when the center of rotation is the bottom right corner (corner 2), would be the same as the image at 91° when the center of rotation is at the bottom left corner (corner 1) of the main pixel. Moreover, it can easily be seen that for the hexagonal grid, at every multiple of 60°, grid will be rotated by the given amount, so the images at a different corner may be observed as the rotated (similar) forms of the original images, without affecting the number of non-bijectivity cases. Figures 4.2 and 4.3 show all possible non-bijective digitized rotations for all three grids. The figure 4.2 shows a bijective digitized rotation by 145° degrees (first image) and a non-bijective one by 45° (second image) on the square grid. A bijective digitized rotation by 69° (third image) and a non-bijective one by 30° (forth image) on the triangular grid. Broken arrows and the solid ones denote the neighbors before and after the digitized rotation, respectively. Non-injective pixels, after the

Table 4.1: Coordinates of main pixel and its closest neighbors and non-bijective angles with respect to all corners in square grid.

Rotation center	Coordinates of main pixel and its neighbors	Non-bijective angles
Corner 1	$(\frac{1}{2},\frac{1}{2}),\quad (\frac{3}{2},\frac{1}{2}),(\frac{1}{2},\frac{3}{2}),(-\frac{1}{2},\frac{1}{2}),(\frac{1}{2},-\frac{1}{2})$	$45°, 315°$
Corner 2	$(-\frac{1}{2},\frac{1}{2}),\quad (\frac{1}{2},\frac{1}{2}),(-\frac{1}{2},\frac{3}{2}),(-\frac{3}{2},\frac{1}{2}),(-\frac{1}{2},-\frac{1}{2})$	$225°, 315°$
Corner 3	$(-\frac{1}{2},-\frac{1}{2}),\quad (\frac{1}{2},-\frac{1}{2}),(-\frac{1}{2},\frac{1}{2}),(-\frac{3}{2},-\frac{1}{2}),(-\frac{1}{2},-\frac{3}{2})$	$135°, 225°$
Corner 4	$(\frac{1}{2},-\frac{1}{2}),\quad (\frac{3}{2},-\frac{1}{2}),(\frac{1}{2},\frac{1}{2}),(-\frac{1}{2},-\frac{1}{2}),(\frac{1}{2},-\frac{3}{2})$	$45°, 135°$

rotations, are shaded in grey color and in the figure 4.3 the top row (left to right) non-bijective angle groups, for integer angles θ, are $\{20°, 21°\}$, $\{22° \leq \theta \leq 25°\}$, $\{95° \leq \theta \leq 98°\}$, $\{99°, 100°\}$ second row (left to right) $\{140°, 141°\}$, $\{142° \leq \theta \leq 145°\}$, $\{215° \leq \theta \leq 218°\}$, $\{219°, 220°\}$ bottom row (left to right), $\{260°, 261°\}$, $\{262° \leq \theta \leq 265°\}$, $\{335° \leq \theta \leq 338°\}$, $\{339°, 340°\}$. Broken arrows denote the neighbors before the digitized rotation whereas the solid ones denote the neighbors after the digitized rotation. Non-injective pixels, after the rotations, are shaded in grey color. Tables 4.1, 4.2, 4.3 and 4.4 give the coordinates of the main pixel and closest neighbors with respect to all possible corners of the main pixel, taken as the rotation center. The tables also provide the non-bijectivity angles or angle intervals for digitized rotations with centers at all possible corners. For the numbering of the corners, please refer to figure 2.5.

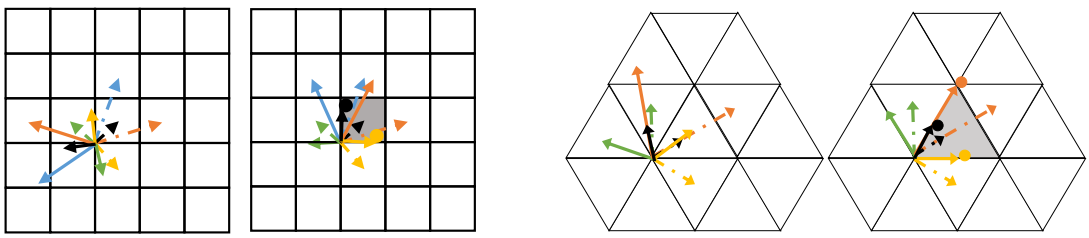

Figure 4.2: A bijective (1st and 3rd figures) and non bijective (2nd and 4th figures) digitized rotations.

Table 4.2: Coordinates of main pixel and its closest neighbors and non-bijective angles with respect to all corners with an even (E) or odd (O) main trixel on triangular grid.

Rotation center	Coordinates of main pixel and closest neighbors	Non-bijective angles
E Corner 1	$(\frac{\sqrt{3}}{2},\frac{1}{2}),$ $(\sqrt{3},1),(0,1),(\frac{\sqrt{3}}{2},-\frac{1}{2})$	$30°, 330°$
E Corner 2	$(-\frac{\sqrt{3}}{2},\frac{1}{2}),$ $(0,1),(-\sqrt{3},1),(-\frac{\sqrt{3}}{2},-\frac{1}{2})$	$210°, 270°$
E Corner 3	$(0,-1),$ $(\frac{\sqrt{3}}{2},-\frac{1}{2}),(-\frac{\sqrt{3}}{2},-\frac{1}{2}),(0,-2)$	$90°, 150°$
O Corner 1	$(0,1),$ $(\frac{\sqrt{3}}{2},\frac{1}{2}),(0,2),(-\frac{\sqrt{3}}{2},\frac{1}{2})$	$270°, 330°$
O Corner 2	$(-\frac{\sqrt{3}}{2},-\frac{1}{2}),$ $(0,-1),(-\frac{\sqrt{3}}{2},\frac{1}{2}),(-\sqrt{3},-1)$	$150°, 210°$
O Corner 3	$(\frac{\sqrt{3}}{2},-\frac{\sqrt{1}}{2}),$ $(\sqrt{3},-1),(\frac{\sqrt{3}}{2},\frac{1}{2}),(0,-1)$	$30°,\ 90°$

Table 4.3: Coordinates of main hexel and its neighbors, with respect to all corners in hexagonal grid.

Rotation Center	Coordinates of main pixel with neighbors
H Corner 1	$(\frac{1}{\sqrt{3}},1),$ $(\frac{4}{\sqrt{3}},2),(\frac{1}{\sqrt{3}},3),(\frac{-2}{\sqrt{3}},2),(\frac{-2}{\sqrt{3}},0),(\frac{1}{\sqrt{3}},-1),(\frac{4}{\sqrt{3}},0)$
H Corner 2	$(\frac{-1}{\sqrt{3}},1),$ $(\frac{2}{\sqrt{3}},2),(\frac{-1}{\sqrt{3}},3),(\frac{-4}{\sqrt{3}},2),(\frac{-4}{\sqrt{3}},0),(\frac{-1}{\sqrt{3}},-1),(\frac{2}{\sqrt{3}},0)$
H Corner 3	$(\frac{-2}{\sqrt{3}},0),$ $(\frac{1}{\sqrt{3}},1),(\frac{-2}{\sqrt{3}},2),(\frac{-5}{\sqrt{3}},1),(\frac{-5}{\sqrt{3}},-1),(\frac{-2}{\sqrt{3}},-2),(\frac{1}{\sqrt{3}},-1)$
H Corner 4	$(\frac{-1}{\sqrt{3}},-1),$ $(\frac{-1}{\sqrt{3}},1),(\frac{-4}{\sqrt{3}},0),(\frac{-4}{\sqrt{3}},-2),(\frac{-1}{\sqrt{3}},-3),(\frac{2}{\sqrt{3}},-2),(\frac{2}{\sqrt{3}},0)$
H Corner 5	$(\frac{1}{\sqrt{3}},-1),$ $(\frac{1}{\sqrt{3}},1),(\frac{-2}{\sqrt{3}},0),(\frac{-2}{\sqrt{3}},-2),(\frac{1}{\sqrt{3}},-3),(\frac{4}{\sqrt{3}},-2),(\frac{4}{\sqrt{3}},0)$
H Corner 6	$(\frac{2}{\sqrt{3}},0),$ $(\frac{-1}{\sqrt{3}},1),(\frac{-1}{\sqrt{3}},-1),(\frac{2}{\sqrt{3}},-2),(\frac{5}{\sqrt{3}},-1),(\frac{5}{\sqrt{3}},1),(\frac{2}{\sqrt{3}},2)$

Table 4.4: Non-bijective angle intervals with respect to all corners in hexagonal grid.

Rotation Center	Non-bijective angle intervals
H Corner 1	$20^\circ \leq \theta \leq 25^\circ, 95^\circ \leq \theta \leq 100^\circ, 140^\circ \leq \theta \leq 145^\circ, 215^\circ \leq \theta \leq 220^\circ,$ $260^\circ \leq \theta \leq 265^\circ, 335^\circ \leq \theta \leq 340^\circ$
H Corner 2	$35^\circ \leq \theta \leq 40^\circ, 80^\circ \leq \theta \leq 85^\circ, 155^\circ \leq \theta \leq 160^\circ, 200^\circ \leq \theta \leq 205^\circ$ $275^\circ \leq \theta \leq 280^\circ, 320^\circ \leq \theta \leq 325^\circ$
H Corner 3	$20^\circ \leq \theta \leq 25^\circ, 95^\circ \leq \theta \leq 100^\circ, 140^\circ \leq \theta \leq 145^\circ, 215^\circ \leq \theta \leq 220^\circ$ $260^\circ \leq \theta \leq 265^\circ, 335^\circ \leq \theta \leq 340^\circ$
H Corner 4	$35^\circ \leq \theta \leq 40^\circ, 80^\circ \leq \theta \leq 85^\circ, 155^\circ \leq \theta \leq 160^\circ, 200^\circ \leq \theta \leq 205^\circ$ $275^\circ \leq \theta \leq 280^\circ, 320^\circ \leq \theta \leq 325^\circ$
H Corner 5	$20^\circ \leq \theta \leq 25^\circ, 95^\circ \leq \theta \leq 100^\circ, 140^\circ \leq \theta \leq 145^\circ, 215^\circ \leq \theta \leq 220^\circ,$ $260^\circ \leq \theta \leq 265^\circ, 335^\circ \leq \theta \leq 340^\circ$
H Corner 6	$35^\circ \leq \theta \leq 40^\circ, 80^\circ \leq \theta \leq 85^\circ, 155^\circ \leq \theta \leq 160^\circ, 200^\circ \leq \theta \leq 205^\circ$ $275^\circ \leq \theta \leq 280^\circ, 320^\circ \leq \theta \leq 325^\circ$

4.3 Rotations around an Edge-midpoint

In this section we consider the rotation center at an edge midpoint. First, let us consider the lower edge midpoint of the main pixel, i.e. the edge midpoint 1-2, referring to figure 2.5. The vectors of the main pixel with neighbors are given in the first rows of tables 4.5, 4.6, 4.8. When the center of the rotation is an edge midpoint, in square grid, we observe that the digitized rotations are injective for all integer angles between 0 and 360 degrees. In hexagonal grid, we have non-injectivity at 13 different integer angles (at 21°, 22°, 23°, 157°, 158°, 159°, 201°, 202°, 203°, 240°, 337°, 338° and 339°) whereas for the triangular grid this number is 38 (all integer angles θ in the intervals $37^\circ \leq \theta \leq 45^\circ$, $135^\circ \leq \theta \leq 143^\circ$, $217^\circ \leq \theta \leq 225^\circ$, $315^\circ \leq \theta \leq 323^\circ$ and at 90° and 270°, for an even main pixel). The pixel loss is 1 in all three grids, but hexagonal grid having more neighbors than the other two grids, gives a better quality in the processed image. For all three grids, we took the center of rotation, first, at the lower edge midpoint; see figure 2.5, and then at other edge midpoints of the main pixel. In [43] we showed that, in the triangular grid, when the center of rotation is an edge midpoint, at every multiple of 60°, we will obtain similar images (rotated by the given angle) at

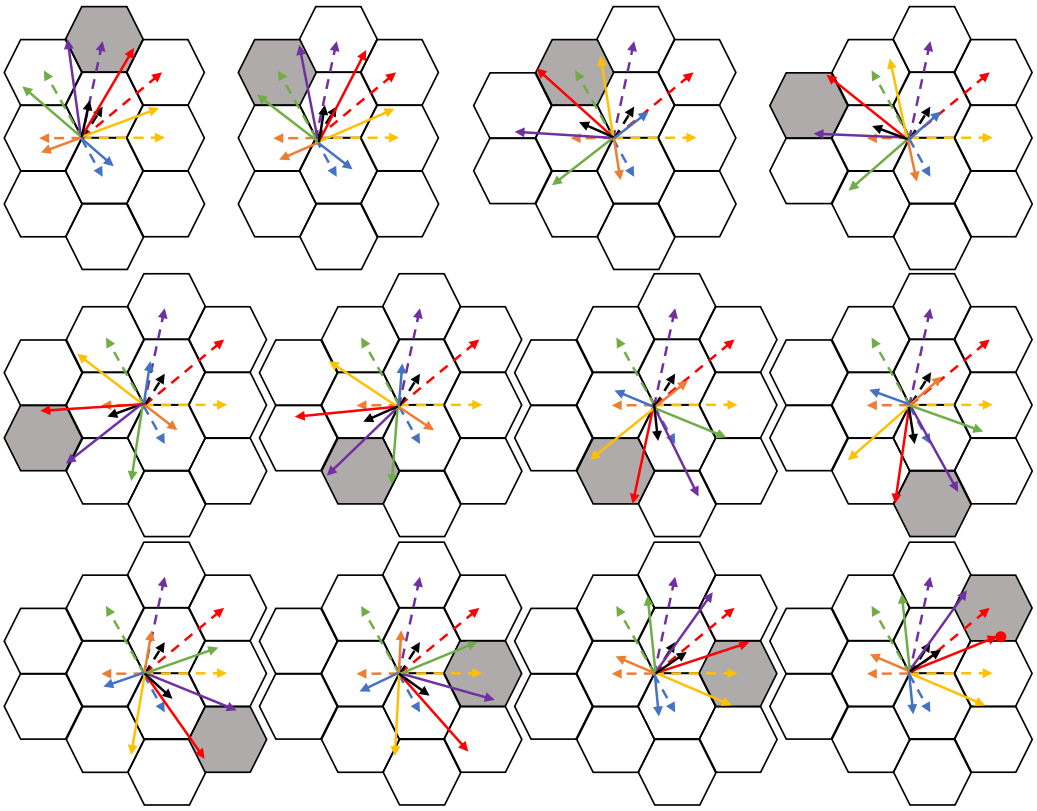

Figure 4.3: All the non-bijective digitized rotations of a main pixel with its closest neighbors on the hexagonal grid, when the center of rotation is the lower left corner point.

a different edge midpoint, without affecting the number of non-bijectivity cases. The images for an odd main trixel can be observed by 180° rotation from the corresponding edge of the even main trixel. Moreover, for the square and the hexagonal grids, due to symmetry, by having the rotation center at other edge midpoint, similar images are obtained as for the lower edge midpoint, but with angles increased/decreased by multiples of 90° and 60°, respectively. For the square grid, each rotation is bijective according to the neighborhood motion map we analyzed. The values for non-bijective angles for the hexagonal grid are shown in table 4.9. Figures 4.4 and 4.5 show all possible non-bijective digitized rotations for the triangular and the hexagonal grids, respectively. In the figure 4.4, top row (left to right) non-bijective angle groups, for integer angles θ, are $\{37^\circ \leq \theta \leq 45^\circ\}, 90^\circ, \{135^\circ \leq \theta \leq 143^\circ\}$ and bottom row (left

to right) $\{217^\circ \leq \theta \leq 225^\circ\}, 270^\circ, \{315^\circ \leq \theta \leq 323^\circ\}$. Broken arrows denote the neighbors before the digitized rotation whereas the solid ones denote the neighbors after the digitized rotation. Non-injective trixels, after the rotations, are shaded in grey color and in the figure 4.5, non-bijective angle groups, for integer angles θ, are $\{21^\circ \leq \theta \leq 23^\circ\}, \{157^\circ \leq \theta \leq 159^\circ\}, \{201^\circ \leq \theta \leq 203^\circ\}, 240^\circ, \{337^\circ \leq \theta \leq 339^\circ\}$. Broken arrows denote the neighbors before the digitized rotation whereas the solid ones denote the neighbors after the digitized rotation. Non-injective hexels, after the rotations, are shaded in grey color. Tables 4.5, 4.6, 4.7, 4.8 and 4.9 give the coordinates of the main pixel and its closest neighbors with respect to all possible edge midpoints of the main pixel, taken as the rotation center. The tables also provide the non-bijectivity angles or angle intervals for digitized rotations with centers at varying edge midpoints. For the labels of edge midpoints, please refer to figure 2.5.

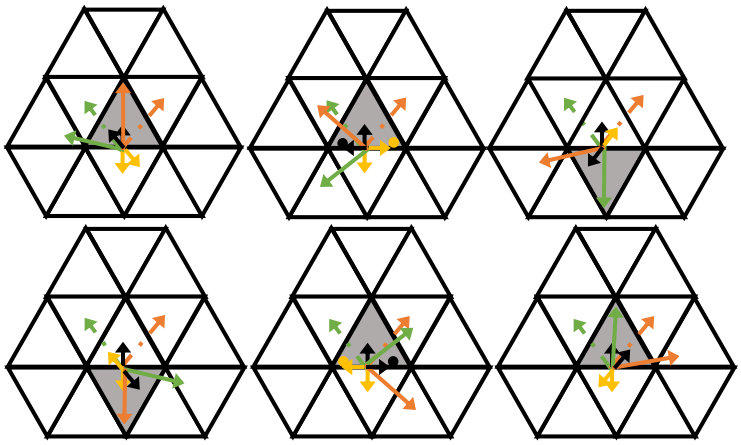

Figure 4.4: All the non-bijective digitized rotations of a main trixel with its closest neighbors on the triangular grid, when the center of rotation is the lower edge midpoint.

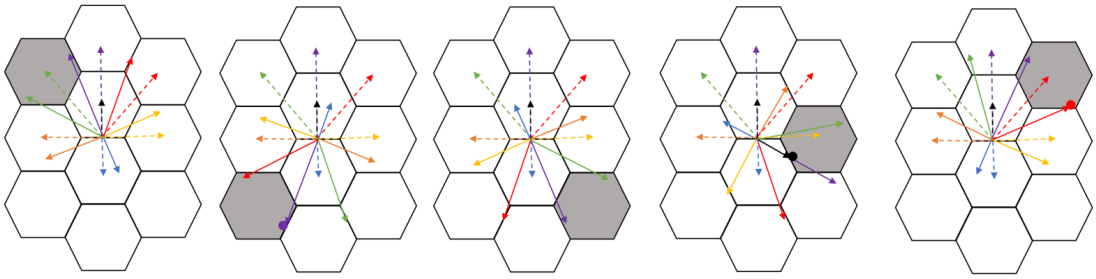

Figure 4.5: All the non-bijective digitized rotations of a main hexel with its closest neighbors on the hexagonal grid, when the center of rotation is the lower edge midpoint.

Table 4.5: Coordinates of main pixel and its closest neighbors with respect to all edge midpoints in square grid.

Rotation center	Coordinates of main pixel and closest neighbors
Edge Mid. 1-2	$(0,\frac{1}{2}),$ $(1,\frac{1}{2}),(0,\frac{3}{2}),(-1,\frac{1}{2}),(0,-\frac{1}{2})$
Edge Mid. 2-3	$(-\frac{1}{2},0),$ $(\frac{1}{2},0),(-\frac{1}{2},1),(-\frac{3}{2},0),(-\frac{1}{2},-1)$
Edge Mid. 3-4	$(0,-\frac{1}{2}),$ $(1,-\frac{1}{2}),(0,\frac{1}{2}),(-1,-\frac{1}{2}),(0,-\frac{3}{2})$
Edge Mid. 4-1	$(\frac{1}{2},0),$ $(\frac{3}{2},0),(\frac{1}{2},1),(-\frac{1}{2},0),(\frac{1}{2},-1)$

Table 4.6: Coordinates of main trixel and its closest neighbors with respect to all edge midpoints for an even and odd main trixel on triangular grid.

Rotation center	Coordinates of main pixel and closest neighbors
Even EM 1-2	$(0,\frac{1}{2}),$ $(\frac{\sqrt{3}}{2},1),(-\frac{\sqrt{3}}{2},1),(0,-\frac{1}{2})$
Even EM 2-3	$(-\frac{\sqrt{3}}{4},-\frac{1}{4}),$ $(\frac{\sqrt{3}}{4},\frac{1}{4}),(-\frac{3\sqrt{3}}{4},\frac{1}{4}),(-\frac{\sqrt{3}}{4},-\frac{5}{4})$
Even EM 1-3	$(\frac{\sqrt{3}}{4},-\frac{1}{4}),$ $(\frac{3\sqrt{3}}{4},\frac{1}{4}),(-\frac{\sqrt{3}}{4},\frac{1}{4}),(\frac{\sqrt{3}}{4},-\frac{5}{4})$
Odd EM 1-2	$(\frac{\sqrt{3}}{4},-\frac{1}{4}),$ $(-\frac{\sqrt{3}}{4},\frac{1}{4}),(-\frac{\sqrt{3}}{4},\frac{5}{4}),(-\frac{3\sqrt{3}}{4},-\frac{1}{4})$
Odd EM 2-3	$(0,\frac{1}{2}),$ $(0,-\frac{1}{2}),(\frac{\sqrt{3}}{2},-1),(-\frac{\sqrt{3}}{2},-1)$
Odd EM 1-3	$(-\frac{\sqrt{3}}{4},-\frac{1}{4}),$ $(\frac{\sqrt{3}}{4},\frac{1}{4}),(\frac{\sqrt{3}}{4},\frac{5}{4}),(\frac{3\sqrt{3}}{4},-\frac{1}{4})$

Table 4.7: Non-bijective angles or angle intervals for all edge midpoints for an even and odd main trixel in triangular grid.

Rotation center	Non-bijective angles or angle intervals
Even EM 1-2	$37^\circ \leq \theta \leq 45^\circ, 90^\circ, 135^\circ \leq \theta \leq 143^\circ$ $217^\circ \leq \theta \leq 225^\circ, 270^\circ, 315^\circ \leq \theta \leq 323^\circ$
Even EM 2-3	$15^\circ \leq \theta \leq 23^\circ, 97^\circ \leq \theta \leq 105^\circ, 150^\circ$ $195^\circ \leq \theta \leq 203^\circ, 277^\circ \leq \theta \leq 285^\circ, 330^\circ$
Even EM 3-1	$30^\circ, 75^\circ \leq \theta \leq 83^\circ, 157^\circ \leq \theta \leq 165^\circ$ $210^\circ, 255^\circ \leq \theta \leq 263^\circ, 337^\circ \leq \theta \leq 345^\circ$
Odd EM 1-2	$30^\circ, 75^\circ \leq \theta \leq 83^\circ, 157^\circ \leq \theta \leq 165^\circ$ $210^\circ, 255^\circ \leq \theta \leq 263^\circ, 337^\circ \leq \theta \leq 345^\circ$
Odd EM 2-3	$37^\circ \leq \theta \leq 45^\circ, 90^\circ, 135^\circ \leq \theta \leq 143^\circ$ $217^\circ \leq \theta \leq 225^\circ, 270^\circ, 315^\circ \leq \theta \leq 323^\circ$
Odd EM 3-1	$15^\circ \leq \theta \leq 23^\circ, 97^\circ \leq \theta \leq 105^\circ, 150^\circ$ $195^\circ \leq \theta \leq 203^\circ, 277^\circ \leq \theta \leq 285^\circ, 330^\circ$

Table 4.8: Coordinates of main hexel and its neighbors, with respect to all edge midpoints in hexagonal grid.

Rotation Center	Coordinates of main pixel with neighbors
H EM 1-2	$(0,1), \quad (\frac{3}{\sqrt{3}},2), (0,3), (\frac{-3}{\sqrt{3}},2), (\frac{-3}{\sqrt{3}},0), (0,-1), (\frac{3}{\sqrt{3}},0)$
H EM 2-3	$(\frac{-3}{2\sqrt{3}},\frac{1}{2}), \quad (\frac{3}{2\sqrt{3}},-\frac{1}{2}), (\frac{3}{2\sqrt{3}},\frac{3}{2}), (\frac{-3}{2\sqrt{3}},\frac{5}{2}), (\frac{-9}{2\sqrt{3}},\frac{3}{2}), (\frac{-9}{2\sqrt{3}},-\frac{1}{2}), (\frac{-3}{2\sqrt{3}},-\frac{3}{2})$
H EM 3-4	$(\frac{-3}{2\sqrt{3}},-\frac{1}{2}), (\frac{3}{2\sqrt{3}},-\frac{3}{2}), (\frac{3}{2\sqrt{3}},\frac{1}{2}), (\frac{-3}{2\sqrt{3}},\frac{3}{2}), (\frac{-9}{2\sqrt{3}},\frac{1}{2}), (\frac{-9}{2\sqrt{3}},-\frac{3}{2}), (\frac{-3}{2\sqrt{3}},-\frac{5}{2})$
H EM 4-5	$(0,-1), \quad (\frac{3}{\sqrt{3}},0), (0,1), (\frac{-3}{\sqrt{3}},0), (\frac{-3}{\sqrt{3}},-2), (0,-3), (\frac{3}{\sqrt{3}},-2)$
H EM 5-6	$(\frac{3}{2\sqrt{3}},-\frac{1}{2}), (\frac{9}{2\sqrt{3}},-\frac{3}{2}), (\frac{9}{2\sqrt{3}},\frac{1}{2}), (\frac{3}{2\sqrt{3}},\frac{3}{2}), (\frac{-3}{2\sqrt{3}},\frac{1}{2}), (\frac{-3}{2\sqrt{3}},-\frac{3}{2}), (\frac{3}{2\sqrt{3}},-\frac{5}{2})$
H EM 6-1	$(\frac{3}{2\sqrt{3}},\frac{1}{2}), \quad (\frac{9}{2\sqrt{3}},-\frac{1}{2}), (\frac{9}{2\sqrt{3}},\frac{3}{2}), (\frac{3}{2\sqrt{3}},\frac{5}{2}), (\frac{-3}{2\sqrt{3}},\frac{3}{2}), (\frac{-3}{2\sqrt{3}},-\frac{1}{2}), (\frac{3}{2\sqrt{3}},-\frac{3}{2})$

Table 4.9: Non-bijective angles or angle intervals with respect to all edge midpoints (taken as rotation center) in hexagonal grid.

Rotation Center	Non-bijective angles/ angle intervals
H EdgeM 1-2	$21° \leq \theta \leq 23°, 157° \leq \theta \leq 159°, 201° \leq \theta \leq 203°$ $240°, 337° \leq \theta \leq 339°$
H EdgeM 2-3	$97° \leq \theta \leq 99°, 141° \leq \theta \leq 143°, 240°$ $277° \leq \theta \leq 279°, 321° \leq \theta \leq 323°$
H EdgeM 3-4	$37° \leq \theta \leq 39°, 60°, 81° \leq \theta \leq 83°$ $217° \leq \theta \leq 219°, 261° \leq \theta \leq 263°$
H EdgeM 4-5	$21° \leq \theta \leq 23°, 60°, 157° \leq \theta \leq 159°$ $201° \leq \theta \leq 203°, 337° \leq \theta \leq 339°$
H EdgeM 5-6	$60°, 97° \leq \theta \leq 99°, 141° \leq \theta \leq 143°$ $277° \leq \theta \leq 279°, 321° \leq \theta \leq 323°$
H EdgeM 6-1	$37° \leq \theta \leq 39°, 81° \leq \theta \leq 83°, 217° \leq \theta \leq 219°$ $240°, 261° \leq \theta \leq 263°$

Chapter 5

APPLICATIONS

In this section we give some applications. First, in Figure 5.1, we show the original E.M.U. logo, then on the left, both on the triangular and square grids in low resolution, consisting of 22 pixels, and on the right, its images on the triangular and square grids, after a digitized rotation by 40 deg. This digitized rotation is injective for the triangular grid, whereas this is not the case for the square grid. Dark blue pixel in Figure 5.1 (right, bottom) shows the non-injective pixel. Later on, in Figure 5.2, we have a heart shape, again in low resolution, consisting of 40 pixels (29 outer purple, and 11 inner green trixels), and its images after digitized rotations by 15 and 72 degrees. The non-injective pixels after the rotations, are shown in 3 different colors; red ones denote the trixels where the two purple trixels are mapped, yellow ones denote the trixels where the two green trixels are mapped, and finally, the dark red pixel contains the image of one purple and one green trixel after the specified digitized rotation.

In this thesis, we studied digitized rotations on the triangular grid, by conversion to triplet coordinates, and then used this approach, to determine the angle which produces the first change in the neighborhood motion map, for a main trixel together with its one neighbors (i.e. after a digitized rotation by certain angle). We also computed the angle which produces the first non-bijective neighborhood motion map, for a main trixel lying on the positive x-axis.

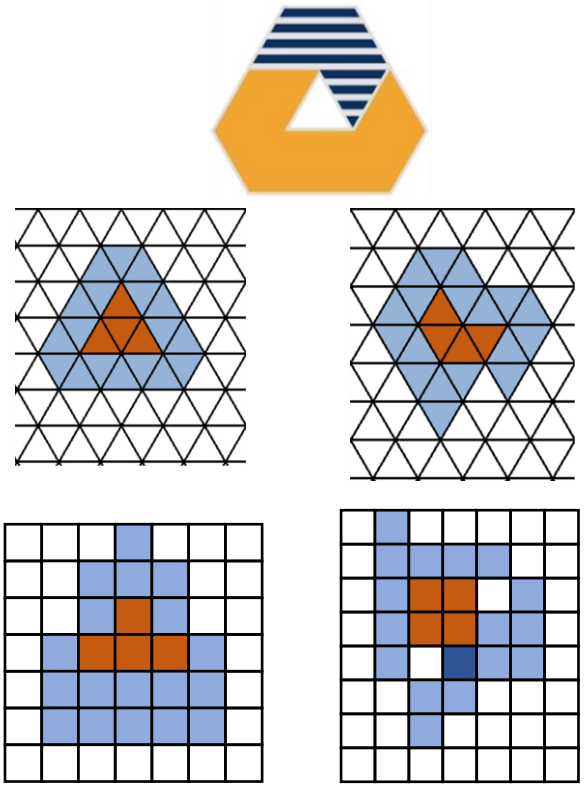

Figure 5.1: The E.M.U. logo and its digitized images

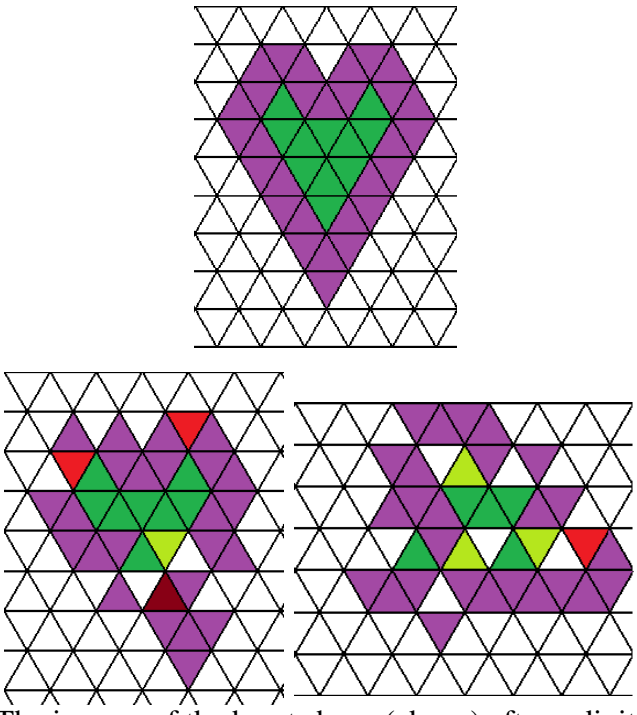

Figure 5.2: The images of the heart shape (above) after a digitized rotation

Chapter 6

CONCLUSIONS

In this thesis we have described bijective digitized rotations of the 12-neighborhood on the triangular grid with various rotation centers in the given main pixel. We believe that our studies, as the first results about rotations on the triangular grid, are helpful for people working on this grid both in theoretical and practical fields. As we have seen the triangular grid shows some advantages over the traditional square grid by counting the number of lost pixels in a neighborhood motion map.

In this thesis, considering only the closest neighbors, we compared the results for the bijectivity of the digitized rotations of the three regular grids. The non-injectivity is important as this notion determines the pixel loss and hence information loss in the processed image. In our experiment, for all three regular grids, we considered digitized rotations (with respect to different rotation centers) for each integer angle between 0 and 360 degrees. In general we have bijectivity at more integer angles for the square and the triangular grids, compared to the hexagonal grid. In case of non-bijectivity, the pixel loss in all three regular grids is 1. The most important quality measure of rotated figures is connected to pixel loss in non-bijective cases. In this thesis the comparison is based on that. However one can also measure the quality of the rotated images in bijective cases based on the concept of digital continuity, [33,44]. One aspect for future study is to investigate this notion of digital continuity, corresponding to rotations. A digitized rigid motion is called digitally continuous if two neighbor pixels still stay neighbors after the motion. When the center of the rotation is the midpoint of a main

pixel, our observation is that triangular grid proves to be digitally continuous at many more integer angles compared to the square grid. We plan to further study this and compare the results among the 3 grids, when the center of rotation is a grid point or midpoint of an edge.

There are various ways to continue the characterization of digitized rotations, e.g., to investigate the bijectivity condition of the local neighborhoods on the triangular grid, when the rotation center is not nearby, but some distance away from the main pixel (and its neighborhood). Already in [42] the authors started to study the digitized rotations of a main trixel with its neighbors when the rotation center is some distance away. One aspect for future work would be to generalize this to a main trixel with all of its 12 neighbors. Another way is to continue the research is to combine rotations with other operations, e.g., translations (described in [19]).

REFERENCES

[1] E. Luczak and A. Rosenfeld, "Distance on a hexagonal grid," *IEEE Transactions on Computers*, vol. C-25, no. 5, pp. 532–533, 1976.

[2] T. Lukić and B. Nagy, "Regularized binary tomography on the hexagonal grid," *Physica Scripta*, vol. 94, no. 2, p. 025201, 2019. [Online]. Available: https://doi.org/10.1088/1402-4896/aafbcb

[3] S. Matej, A. Vardi, G. T. Herman, and E. Vardi, *Binary Tomography Using Gibbs Priors*. Boston, MA: Birkhäuser Boston, 1999, pp. 191–212. [Online]. Available: https://doi.org/10.1007/978-1-4612-1568-4_8

[4] P. Kardos and K. Palágyi, "On topology preservation of mixed operators in triangular, square, and hexagonal grids," *Discret. Appl. Math.*, vol. 216, pp. 441–448, 2017.

[5] P. Kardos and K. Palágyi, "Unified characterization of p-simple points in triangular, square, and hexagonal grids," in *Computational Modeling of Objects Presented in Images. Fundamentals, Methods, and Applications - 5th International Symposium, CompIMAGE 2016, Niagara Falls, NY, USA, September 21-23, 2016, Revised Selected Papers*, ser. Lecture Notes in Computer Science, R. P. Barneva, V. E. Brimkov, and J. M. R. S. Tavares, Eds., vol. 10149, 2016, pp. 79–88. [Online]. Available: https://doi.org/10.1007/978-3-319-54609-4_6

[6] E. S. Deutsch, “Thinning algorithms on rectangular, hexagonal, and triangular arrays,” *Commun. ACM*, vol. 15, no. 9, p. 827–837, 1972. [Online]. Available: https://doi.org/10.1145/361573.361583

[7] K. Pluta, P. Romon, Y. Kenmochi, and N. Passat, “Bijective rigid motions of the 2d cartesian grid,” in *Discrete Geometry for Computer Imagery - 19th IAPR International Conference, DGCI 2016, Nantes, France, April 18-20, 2016. Proceedings*, ser. Lecture Notes in Computer Science, N. Normand, J. V. Guédon, and F. Autrusseau, Eds., vol. 9647. Springer, 2016, pp. 359–371. [Online]. Available: https://doi.org/10.1007/978-3-319-32360-2_28

[8] ——, “Honeycomb geometry: Rigid motions on the hexagonal grid,” in *Discrete Geometry for Computer Imagery - 20th IAPR International Conference, DGCI 2017, Vienna, Austria, September 19-21, 2017, Proceedings*, ser. Lecture Notes in Computer Science, W. G. Kropatsch, N. M. Artner, and I. Janusch, Eds., vol. 10502. Springer, 2017, pp. 33–45. [Online]. Available: https://doi.org/10.1007/978-3-319-66272-5_4

[9] L. Middleton and J. Sivaswamy, *Hexagonal Image Processing: A Practical Approach*, 2005.

[10] B. Nagy and T. Lukic, “Dense projection tomography on the triangular tiling,” *Fundamenta Informaticae*, vol. 145, pp. 125–141, 2016.

[11] B. Nagy and E. V. Moisi, “Binary tomography on the triangular grid with 3 alternative directions - A genetic approach,” in *22nd International Conference*

on Pattern Recognition, ICPR 2014, Stockholm, Sweden, August 24-28, 2014. IEEE Computer Society, 2014, pp. 1079–1084. [Online]. Available: https://doi.org/10.1109/ICPR.2014.195

[12] ——, "Memetic algorithms for reconstruction of binary images on triangular grids with 3 and 6 projections," *Applied Soft Computing*, vol. 52, pp. 549–565, 2017. [Online]. Available: https://www.sciencedirect.com/science/article/pii/S1568494616305270

[13] B. Nagy, "Distances with neighborhood sequences in cubic and triangular grids," *Pattern Recognition Letters*, vol. 28, pp. 99–109, 2007.

[14] G. Kovács, B. Nagy, and B. Vizvári, "An integer programming approach to characterize digital disks on the triangular grid," in *Discrete Geometry for Computer Imagery - 20th IAPR International Conference, DGCI 2017, Vienna, Austria, September 19-21, 2017, Proceedings*, ser. Lecture Notes in Computer Science, W. G. Kropatsch, N. M. Artner, and I. Janusch, Eds., vol. 10502. Springer, 2017, pp. 94–106. [Online]. Available: https://doi.org/10.1007/978-3-319-66272-5_9

[15] B. Nagy, "Characterization of digital circles in triangular grid," *Pattern Recognition Letters*, vol. 25, pp. 1231–1242, 2004.

[16] B. Nagy and K. Barczi, "Isoperimetrically optimal polygons in the triangular grid with jordan-type neighbourhood on the boundary," *International Journal*

of Computer Mathematics, vol. 90, no. 8, pp. 1629–1652, 2013. [Online]. Available: https://doi.org/10.1080/00207160.2012.737914

[17] M. Abdalla and B. Nagy, "Dilation and erosion on the triangular tessellation: An independent approach," *IEEE Access*, vol. 6, pp. 23 108–23 119, 2018.

[18] M. Saadat and B. Nagy, "Cellular automata approach to mathematical morphology in the triangular grid," *Acta Polytechnica Hungarica*, vol. 15, pp. 45–62, 2018.

[19] K. Abuhmaidan and B. Nagy, "Non-bijective translations on the triangular plane," in *2018 IEEE 16th World Symposium on Applied Machine Intelligence and Informatics (SAMI)*, 2018, pp. 000 183–000 188.

[20] P. Kardos and K. Palágyi, "Topology preservation on the triangular grid," *Annals of Mathematics and Artificial Intelligence*, vol. 75, pp. 53–68, 2014.

[21] M. Dutt, E. Andres, and G. Largeteau-Skapin, "Characterization and generation of straight line segments on triangular cell grid," *Pattern Recognit. Lett.*, vol. 103, pp. 68–74, 2018. [Online]. Available: https://doi.org/10.1016/j.patrec.2018.01.009

[22] H. M. M. Sadeghi and B. Nagy, "On the chamfer polygons on the triangular grid," in *Combinatorial Image Analysis - 18th International Workshop, IWCIA 2017, Plovdiv, Bulgaria, June 19-21, 2017, Proceedings*, ser. Lecture Notes in Computer Science, V. E. Brimkov and R. P.

Barneva, Eds., vol. 10256. Springer, 2017, pp. 53–65. [Online]. Available: https://doi.org/10.1007/978-3-319-59108-7_5

[23] B. Nagy, "Isometric transformations of the dual of the hexagonal lattice," in *2009 Proceedings of 6th International Symposium on Image and Signal Processing and Analysis*, 2009, pp. 432–437.

[24] B. Nouvel and E. Rémila, "On colorations induced by discrete rotations," in *Discrete Geometry for Computer Imagery, 11th International Conference, DGCI 2003, Naples, Italy, November 19-21, 2003, Proceedings*, ser. Lecture Notes in Computer Science, I. Nyström, G. S. di Baja, and S. Svensson, Eds., vol. 2886. Springer, 2003, pp. 174–183. [Online]. Available: https://doi.org/10.1007/978-3-540-39966-7_16

[25] B. Nouvel and E. Remila, "Configurations induced by discrete rotations: Periodicity and quasi-periodicity properties," *Discrete Applied Mathematics*, vol. 147, pp. 325–343, 2005.

[26] A. Avkan, B. Nagy, and M. Saadetoğlu, "Digitized rotations of 12 neighbors on the triangular grid," *Ann. Math. Artif. Intell.*, vol. 88, no. 8, pp. 833–857, 2020. [Online]. Available: https://doi.org/10.1007/s10472-019-09688-w

[27] Y. Thibault, "Rotations in 2D and 3D discrete spaces," Theses, Université Paris-Est, 2010. [Online]. Available: https://pastel.archives-ouvertes.fr/tel-00596947

[28] A. E. Kaufman, "Voxels as a computational representation of geometry," in *in*

The Computational Representation of Geometry. SIGGRAPH '94 Course Notes, 1994, p. 45.

[29] G. Borgefors, "Distance transformations in hexagonal grids," *NASA STI/Recon Technical Report A*, vol. 89, p. 12603, 1987.

[30] M. J. E. Golay, "Hexagonal parallel pattern transformations," *IEEE Trans. Computers*, vol. 18, no. 8, pp. 733–740, 1969. [Online]. Available: https://doi.org/10.1109/T-C.1969.222756

[31] G. Herman and A. Kuba, *Discrete Tomography: Foundations, Algorithms, and Applications*, 1999.

[32] B. Nagy, "Cellular topology and topological coordinate systems on the hexagonal and on the triangular grids," *Annals of Mathematics and Artificial Intelligence*, vol. 75, pp. 117–134, 2014.

[33] K. Abuhmaidan and B. Nagy, "Bijective, non-bijective and semi-bijective translations on the triangular plane," *Mathematics*, vol. 8, no. 1, 2020. [Online]. Available: https://www.mdpi.com/2227-7390/8/1/29

[34] G. Kovács, B. Nagy, and B. Vizvári, "Chamfer distances on the isometric grid: a structural description of minimal distances based on linear programming approach," *J. Comb. Optim.*, vol. 38, no. 3, pp. 867–886, 2019. [Online]. Available: https://doi.org/10.1007/s10878-019-00425-x

[35] E. Andres, “Discrete circles, rings and spheres,” *Computers & Graphics*, vol. 18, no. 5, pp. 695–706, 1994. [Online]. Available: https://www.sciencedirect.com/science/article/pii/0097849394901643

[36] B. Nouvel and E. Rémila, “Characterization of bijective discretized rotations,” in *Combinatorial Image Analysis, 10th International Workshop, IWCIA 2004, Auckland, New Zealand, December 1-3, 2004, Proceedings*, ser. Lecture Notes in Computer Science, R. Klette and J. D. Zunic, Eds., vol. 3322. Springer, 2004, pp. 248–259. [Online]. Available: https://doi.org/10.1007/978-3-540-30503-3_19

[37] A. Avkan, B. Nagy, and M. Saadetoglu, “A comparison of digitized rotations of neighborhood motion maps of closest neighbors on 2d regular grids,” *Signal Image Video Process.*, vol. 16, no. 2, pp. 505–513, 2022. [Online]. Available: https://doi.org/10.1007/s11760-021-01993-4

[38] I. Her, “A symmetrical coordinate frame on the hexagonal grid for computer graphics and vision,” *Journal of Mechanical Design*, vol. 115, pp. 447–449, 1993.

[39] I. Stojmenovic, “Honeycomb networks: Topological properties and communication algorithms,” *Parallel and Distributed Systems, IEEE Transactions on*, vol. 8, pp. 1036 – 1042, 1997.

[40] I. Her, “Geometric transformations on the hexagonal grid,” *IEEE Transactions on Image Processing*, vol. 4, no. 9, pp. 1213–1222, 1995.

[41] B. Nagy, “Finding shortest path with neighbourhood sequences in triangular

grids," *ISPA 2001. Proceedings of the 2nd International Symposium on Image and Signal Processing and Analysis. In conjunction with 23rd International Conference on Information Technology Interfaces (IEEE Cat.)*, pp. 55–60, 2001.

[42] A. Avkan, B. Nagy, and M. Saadetoğlu, "On the angles of change of the neighborhood motion maps on the triangular grid," in *11th International Symposium on Image and Signal Processing and Analysis, ISPA 2019, Dubrovnik, Croatia, September 23-25, 2019*, S. Loncaric, R. Bregovic, M. Carli, and M. Subasic, Eds. IEEE, 2019, pp. 76–81. [Online]. Available: https://doi.org/10.1109/ISPA.2019.8868526

[43] A. Avkan, B. Nagy, and M. Saadetoglu, "Digitized rotations of closest neighborhood on the triangular grid," in *Combinatorial Image Analysis - 19th International Workshop, IWCIA 2018, Porto, Portugal, November 22-24, 2018, Proceedings*, ser. Lecture Notes in Computer Science, R. P. Barneva, V. E. Brimkov, and J. M. R. S. Tavares, Eds., vol. 11255. Springer, 2018, pp. 53–67. [Online]. Available: https://doi.org/10.1007/978-3-030-05288-1_5

[44] A. Rosenfeld, "'Continuous' functions on digital pictures," *Pattern Recognition Letters*, vol. 4, pp. 177–184, 1986.